Contents

1 MC samples and selection **1**

1.1 Data and MC samples . . . 1

1.1.1 MC samples and cross-sections . . . 1

1.2 Multijet background . . . 8

1.3 Z vertex reweighting . . . 13

1.4 W analysis event selection and control plots . . . 13

1.4.1 Event selection . . . 14

1.4.2 $\sqrt{s} = 13$ TeV dataset control plots . . . 14

1.4.3 $\sqrt{s} = 5$ TeV dataset control plots . . . 24

Bibliography . . . 31

List of Figures

11 Distributions for the 5 TeV low-μ dataset in a $Z/\gamma^* \to \mu\mu$ (top row) and a $Z/\gamma^* \to ee$ (bottom row) selection. The data (points) is compared to $Z/\gamma^* \to \mu\mu$ or $Z/\gamma^* \to ee$ signal MC, respectively. The left and middle plots show the actual μ in a coarsely-binned and a finely-binned version. The right plot shows the number of reconstructed primary vertices N_{PV} . . . 2

12 Distributions for the 13 TeV low-μ datasets taken in 2017 and 2018 in a $Z/\gamma^* \to \mu\mu$ (top row) and a $Z/\gamma^* \to ee$ (bottom row) selection. The data (points) is compared to $Z/\gamma^* \to \mu\mu$ or $Z/\gamma^* \to ee$ signal MC, respectively. All distributions are (roughly) normalised to the same number of selected events in the 2017 dataset. The left and middle plots show the actual μ in a coarsely-binned and a finely-binned version. The right plot shows the number of reconstructed primary vertices N_{PV}. 2

13 $< u_{\parallel}^{\ell} >$ as a function of ptcone20, before and after correction using data samples at $\sqrt{s}$ = 13 TeV. 10

14 Extrapolation of the multijet distributions for the lepton transverse momentum (top) and pseudo-rapidity (bottom), in the $W^+ \to e^+\nu$ (left) and $W^+ \to \mu^+\nu$ (right) channels at $\sqrt{s}$ = 13 TeV 11

15 Extrapolation of the multijet distributions for the missing transverse energy (top) and transverse mass (bottom), in the $W^+ \to e^+\nu$ (left) and $W^+ \to \mu^+\nu$ (right) channels at $\sqrt{s}$ = 13 TeV 12

16 Distributions for the 5 TeV (left) and 13 TeV (right) low-μ dataset(s) in a $Z/\gamma^* \to \mu\mu$ (top row) and a $Z/\gamma^* \to ee$ (bottom row) selection. The data (points) is compared to $Z/\gamma^* \to \mu\mu$ or $Z/\gamma^* \to ee$ signal MC, respectively. The distributions of the z-position of the primary vertex selected as the hard interaction are compared for the dataset(s) and the MC simulation before ("no z_{vtx} rwgt", blue, only 13 TeV) and after reweighting (black). For the 13 TeV data the 2017 and 2018 data are shown separately and all distributions are (roughly) normalised to the same number of selected events in the 2017 dataset. 13

17 $\Sigma\vec{E}_T$ distribution in the muon and electron channel for the $\sqrt{s}$ = 13 TeV dataset. 17

18 ΣE_T distribution in the muon and electron channel for the $\sqrt{s}$ = 13 TeV dataset. 18

19 $\vec{E}_T^{miss}$ distribution in the muon and electron channel for the $\sqrt{s}$ = 13 TeV dataset. 19

110 Transverse mass distribution of the W boson in the muon and electron channel for the $\sqrt{s}$ = 13 TeV dataset. 20

111 Lepton pseudorapidity distribution in the muon and electron channel for the $\sqrt{s}$ = 13 TeV dataset. 21

112 Lepton transverse momentum distribution in the muon and electron channel for the $\sqrt{s}$ = 13 TeV dataset. 22

113 W transverse momentum distribution in the muon and electron channel for the $\sqrt{s}$ = 13 TeV dataset. 23

114 $\Sigma\vec{E}_T$ distribution in the muon and electron channel for the $\sqrt{s}$ = 5 TeV dataset. 24

115 ΣE_T distribution in the muon and electron channel for the $\sqrt{s}$ = 5 TeV dataset. 25

116 $\vec{E}_T^{miss}$ distribution in the muon and electron channel for the $\sqrt{s}$ = 5 TeV dataset. 26

117 Transverse mass distribution of the W boson in the muon and electron channel for the $\sqrt{s}$ = 5 TeV dataset. 27

118 Lepton pseudorapidity distribution in the muon and electron channel for the $\sqrt{s}$ = 5 TeV dataset. 28

119 Lepton transverse momentum distribution in the muon and electron channel for the $\sqrt{s}$ = 5 TeV dataset. . . . 29
120 W transverse momentum distribution in the muon and electron channel for the $\sqrt{s}$ = 5 TeV dataset. . . . 30

List of Tables

11 Monte Carlo samples at $\sqrt{s}$ = 13TeV. Given is a short description of the process, the ATLAS MC data set number (DSID), the names and version numbers of the MC generator(s), the used value of the higher order cross section times any branching and filter efficiencies (σ·BR·ϵ_{filter}) with the theoretical uncertainty in percent ("th. unc."), and finally the number of events analysed after skimming at derivation production ($N_{\text{evt}}^{\text{skim}}$) as well as the number of events originally processed and simulated ($N_{\text{evt}}^{\text{unskim}}$). In the case of $Z \to \ell\ell$ samples, the given $\epsilon_{\text{filter}} > 1$ is related to the fact, that the cross sections were calculated for $66 < m_{\ell\ell} < 116$GeV, but the generated mass range is larger. The last section of $t\bar{t}$ samples refers to variation samples for systematics studies. The MC equivalent luminosity $N_{\text{evt}}^{\text{unskim}}/(\sigma\text{·BR·}\epsilon_{\text{filter}})$ is generally above 3fb^{-1} for signal and significant backgrounds, the exception are Powheg $W \to \tau\nu$ and $Z \to \tau\tau$ samples, that have about 0.45fb^{-1} only. . . . 4
12 Alternative signal $Z \to \ell\ell$ Monte Carlo samples at $\sqrt{s}$ = 13TeV produced with Sherpa. General description of the table see Table 11. The samples are split into a long list of orthogonal slices based on "max(pTV,HT)" and filtered further into "b/c/light-jet" subcomponents. For the purpose of this analysis, the number of events in each slice is such that the samples are about 2fb^{-1} each (after application of a penalty factor for negative weight events) and an "inclusive sample" is restored after merging the slices. . . . 5
13 Alternative signal $W \to \ell\nu$ Monte Carlo samples at $\sqrt{s}$ = 13TeV produced with Sherpa. See Table 12 for a description of the table. The samples are split into a long list of orthogonal slices based on "max(pTV,HT)" and filtered further into "b/c/light-jet" subcomponents. For the purpose of this analysis, the number of events in each slice is such that the samples are about 1fb^{-1} each (after application of a penalty factor for negative weight events) and an "inclusive sample" is restored after merging the slices. . . . 6
14 Monte Carlo samples at $\sqrt{s}$ = 5TeV. The table follows the same format as Table 11. The MC equivalent luminosity $N_{\text{evt}}^{\text{unskim}}/(\sigma\text{·BR·}\epsilon_{\text{filter}})$ is generally above 2.5fb^{-1} for signal and significant backgrounds, the exception are Powheg $W \to \tau\nu$ and $Z \to \tau\tau$ samples, that have about 0.20fb^{-1} and 0.45fb^{-1} only. . . . 7

15 Analysis cut flow for $W^+ \to e^+\nu$ 5 TeV signal selection. Lepton p_T is required to be over 18 GeVbefore the final cut. 14
16 Analysis cut flow for $W^+ \to e^+\nu$ 13 TeV signal selection. Lepton p_T is required to be over 18 GeVbefore the final cut. 15
17 Analysis cut flow for $W^+ \to \mu^+\nu$ 5 TeV signal selection. Lepton p_T is required to be over 18 GeVbefore the final cut. 15
18 Analysis cut flow for $W^+ \to \mu^+\nu$ 13 TeV signal selection. Lepton p_T is required to be over 18 GeVbefore the final cut. 15
19 Analysis cut flow for $W^- \to e^-\nu$ 5 TeV signal selection. Lepton p_T is required to be over 18 GeVbefore the final cut. 16
110 Analysis cut flow for $W^- \to e^-\nu$ 13 TeV signal selection. Lepton p_T is required to be over 18 GeVbefore the final cut. 16
111 Analysis cut flow for $W^- \to \mu^-\nu$ 5 TeV signal selection. Lepton p_T is required to be over 18 GeVbefore the final cut. 16
112 Analysis cut flow for $W^- \to \mu^-\nu$ 13 TeV signal selection. Lepton p_T is required to be over 18 GeVbefore the final cut. 16
113 Observed and Expected yield comparison for all signal selections. 17

1 MC samples and selection

"Potentielle citation sans aucun rapport avec le sujet"

— Personne inconnue, *contexte à déterminer*

1.1 Data and MC samples

The data and MC samples for this study were collected under special beam conditions that ensure low pile-up. The data samples were collected in three runs:

- $\sqrt{s}$ = 5.02TeV data taken in November 2017, ATLAS data period M, preliminary calibrated luminosity 256.827 pb^{-1} with an uncertainty of ±1.6%
- $\sqrt{s}$ = 13TeV data taken in November 2017, ATLAS data period N, preliminary online luminosity 146.6pb^{-1}
- $\sqrt{s}$ = 13TeV data taken in June 2018, ATLAS data period G4+J, preliminary online luminosity 193.2pb^{-1}

The runs of November 2017 and the run of June 2018 had the same bunch spacing of 25 ns, but a different filling scheme. The two main differences from the high-μ data collection are the following:

- In order to optimize topo-cluster response for the Hadronic Recoil (HR) lower topo-cluster thresholds were used.
- Single e and μ triggers with significantly lower thresholds and looser identification criteria are run without prescale, most notably `HLT_e15_lhloose_nod0_L1EM12` and `HLT_mu14`.

At the beginning of 5 TeV fills the pile-up reached $\mu\backslash 5$, slowly descending to $\mu\backslash 1$ by the end of the run. In the case of 13 TeV the luminosity was levelled at $\mu = 2$ in the course of the run. The corresponding distributions for μ and N_{PV} for the 5 TeV and 13 TeV runs are shown in Fig. 11 and Fig. 12.

1.1.1 MC samples and cross-sections

Signal and background processes are modelled using fully simulated and reconstructed using Monte-Carlo (MC) samples, specifically tuned for the special run conditions, namely the pileup conditions,

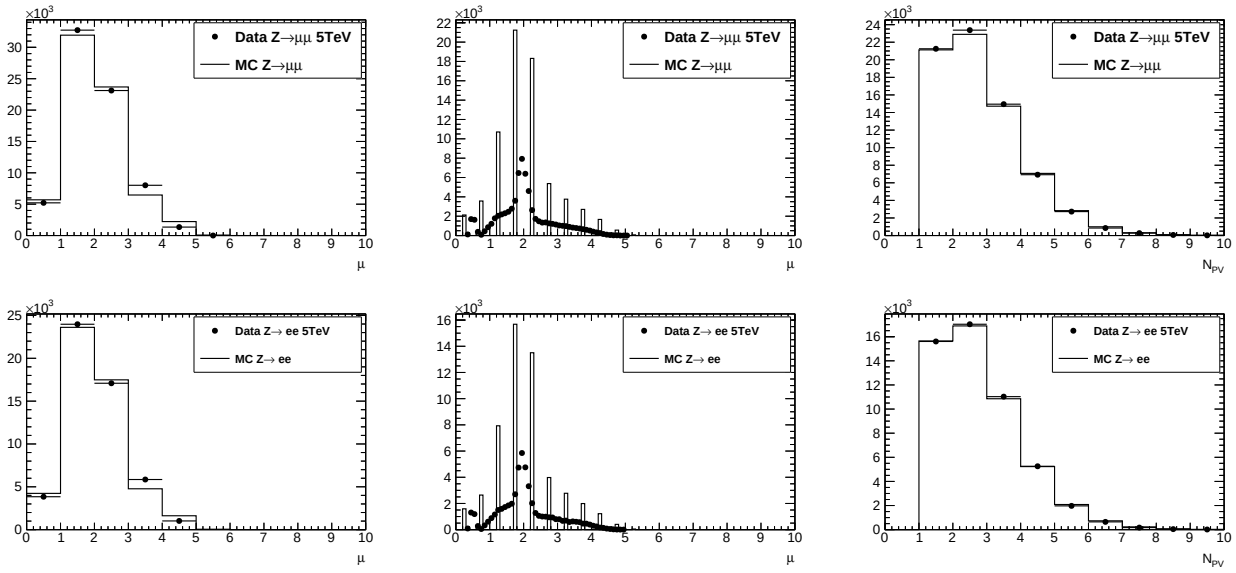

Figure 11: Distributions for the 5 TeV low-μ dataset in a $Z/\gamma^* \to \mu\mu$ (top row) and a $Z/\gamma^* \to ee$ (bottom row) selection. The data (points) is compared to $Z/\gamma^* \to \mu\mu$ or $Z/\gamma^* \to ee$ signal MC, respectively. The left and middle plots show the actual μ in a coarsely-binned and a finely-binned version. The right plot shows the number of reconstructed primary vertices N_{PV}.

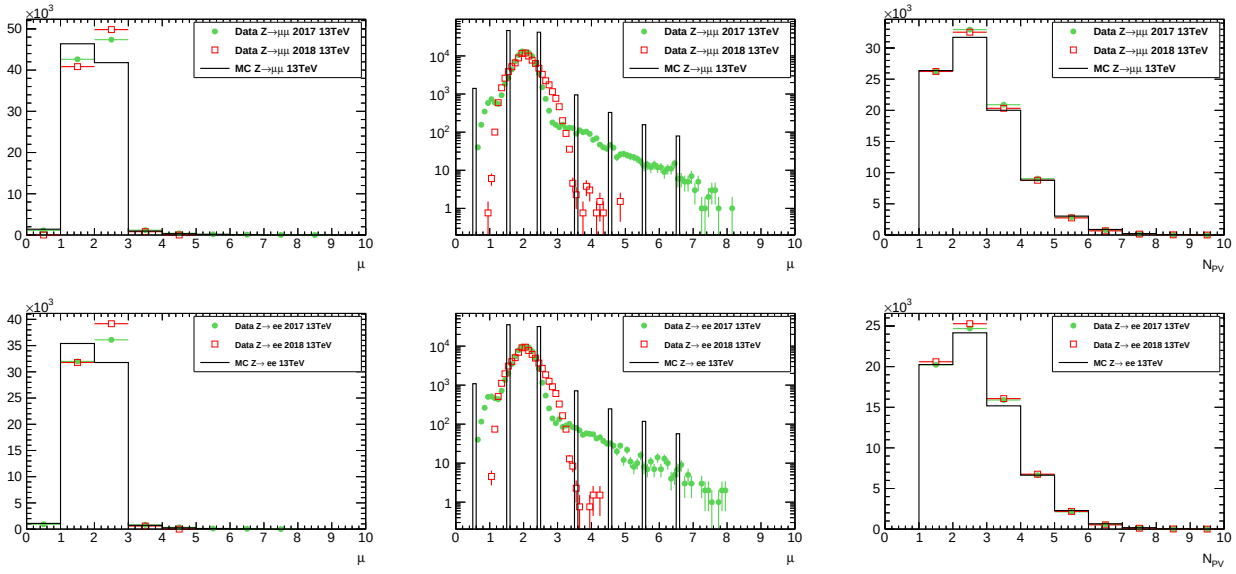

Figure 12: Distributions for the 13 TeV low-μ datasets taken in 2017 and 2018 in a $Z/\gamma^* \to \mu\mu$ (top row) and a $Z/\gamma^* \to ee$ (bottom row) selection. The data (points) is compared to $Z/\gamma^* \to \mu\mu$ or $Z/\gamma^* \to ee$ signal MC, respectively. All distributions are (roughly) normalised to the same number of selected events in the 2017 dataset. The left and middle plots show the actual μ in a coarsely-binned and a finely-binned version. The right plot shows the number of reconstructed primary vertices N_{PV}.

lower topo-cluster noise thresholds and adapter trigger menu. No pileup reweighting is performed. The information on the simulated samples and their properties is given in Tables 11, 12, 13, 14 [1]. The predicted event counts are normalized to the cross-sections quoted in the table.
The primary signal event samples for W and Z production are obtained using Powheg [2, 3, 4, 5] event generator with CT10 PDF, linked with Pythia8 [6] with AZNLO tune [7]. Powheg+Pythia88 samples are interfaced to Photos++ [8] for final state Quantum Electrodynamics (QED) effects simulation.
A set of alternative samples at $\sqrt{s}$ = 13TeV was prepared with Sherpa2.2.2 [9] using the NNPDF3.0 PDFs and merging $V+0,1,2$ at NLO accuracy with $V+3,4$ at LO accuracy with the MEPS@NLO scheme.
A similar set for $\sqrt{s}$ = 5TeV was prepared with Sherpa2.2.5 with a setup similar to 13 TeV samples.
Pileup is modelled by overlaying simulated soft events over the original hard-scattering event. These soft events were modelled using Pythia8 with NNPDF2.3LO set of PDFs [10] and the A3 tune [11].
The W and Z processes samples are normalized to NNLO calculations performed using the DYTURBO, an optimised version of DYNNLO [12, 13] using the MMHT2014nnlo PDF set [14]. Corresponding numerical values were taken from the corresponding ATLAS publications of the 2015 data at 13 TeV [15] and 5.02 TeV [16] are presented in Table 11 for 13 TeV and Table 14 for 5 TeV. The uncertainties on those cross-sections arise from the choice of PDF set, from factorization and renormalisation scale dependence, and the strong coupling constant α_s uncertainty resulting in the total uncertainty estimate of 5%.

Backgrounds from top-quark pair-production $t\bar{t}$ and single-top production (Wt, t-channel, s-channel) were generated with Powheg+Pythia8. The 5 TeV $t\bar{t}$ cross section is taken as the top++ prediction observed by CMS [17]. Di-boson combinations $VV, V = W, Z$ are generated with Sherpa in all decay channels with a requirement of having at least one real lepton in the final state.

Process	Data set	Generator	σ·BR·ϵ_{filter} [nb] (th. unc.)	$N_{\text{evt}}^{\text{skim}}$ [10^6]	$N_{\text{evt}}^{\text{unskim}}$ [10^6]
$W^+ \to e^+\nu$	361100	Powheg+Pythia8	11.61 (5%)	40	40
$W^+ \to \mu^+\nu$	361101	Powheg+Pythia8	11.61 (5%)	40	40
$W^+ \to \tau^+\nu$	361102	Powheg+Pythia8	11.61 (5%)	0.28	5.0
$W^- \to e^-\bar{\nu}$	361103	Powheg+Pythia8	8.630 (5%)	30	30
$W^- \to \mu^-\bar{\nu}$	361104	Powheg+Pythia8	8.630 (5%)	29	29
$W^- \to \tau^-\bar{\nu}$	361105	Powheg+Pythia8	8.630 (5%)	0.24	4.0
$Z \to ee$	361106	Powheg+Pythia8	1.910 × 1.03 (5%)	10	10
$Z \to \mu\mu$	361107	Powheg+Pythia8	1.910 × 1.025 (5%)	10	10
$Z \to \tau\tau$	361108	Powheg+Pythia8	1.910 × 1.025 (5%)	0.12	1.0
$ZZ(q\bar{q}\ell\ell)$	363356	Sherpa 2.2.1	0.01556 × 0.141 (10%)	0.0064	0.010
$WZ(q\bar{q}\ell\ell)$	363358	Sherpa 2.2.1	0.003433 (10%)	0.0063	0.010
$WW(q\bar{q}\ell\nu)$	363359	Sherpa 2.2.1	0.02472 (10%)	0.0093	0.020
$WW(\ell\nu q\bar{q})$	363360	Sherpa 2.2.1	0.02472 (10%)	0.0093	0.020
$WZ(\ell\nu q\bar{q})$	363489	Sherpa 2.2.1	0.01142 (10%)	0.0047	0.010
$ZZ(4\ell)$	364250	Sherpa 2.2.2	0.001252 (10%)	0.0057	0.010
$WZ(3\ell\nu)$	364253	Sherpa 2.2.2	0.004583 (10%)	0.0062	0.010
$WW(2\ell 2\nu)$	364254	Sherpa 2.2.2	0.01250 (10%)	0.0073	0.010
$WZ(\ell 3\nu)$	364255	Sherpa 2.2.2	0.003235 (10%)	0.0050	0.010
Wt	410013	Powheg+Pythia8	0.03582 (10%)	0.0037	0.010
$W\bar{t}$	410014	Powheg+Pythia8	0.03399 (10%)	0.0037	0.010
$t\bar{t}$ (nominal)	410470	Powheg+Pythia8	0.8318 × 0.544 (7%)	1.2	2.0
t(t − chan.t)	410642	Powheg+Pythia8	0.03699 (10%)	0.016	0.030
t(t − chan.$\bar{t}$)	410643	Powheg+Pythia8	0.02217 (10%)	0.011	0.020
t(s − chan.t)	410644	Powheg+Pythia8	0.002027 (10%)	0.0050	0.010
t(s − chan.$\bar{t}$)	410645	Powheg+Pythia8	0.001268 (10%)	0.0052	0.010
$t\bar{t}$ (syst.)	410480	Powheg+Pythia8	0.8318 × 0.438 (7%)	0.85	1.5
$t\bar{t}$ (syst.)	410482	Powheg+Pythia8	0.8318 × 0.105 (7%)	0.40	0.50
$t\bar{t}$ (syst.)	410557	Powheg+Pythia8	0.8318 × 0.438 (7%)	0.85	1.5
$t\bar{t}$ (syst.)	410558	Powheg+Pythia8	0.8318 × 0.105 (7%)	0.40	0.50

Table 11: Monte Carlo samples at $\sqrt{s}$ = 13TeV. Given is a short description of the process, the ATLAS MC data set number (DSID), the names and version numbers of the MC generator(s), the used value of the higher order cross section times any branching and filter efficiencies (σ·BR·ϵ_{filter}) with the theoretical uncertainty in percent ("th. unc."), and finally the number of events analysed after skimming at derivation production ($N_{\text{evt}}^{\text{skim}}$) as well as the number of events originally processed and simulated ($N_{\text{evt}}^{\text{unskim}}$). In the case of $Z \to \ell\ell$ samples, the given $\epsilon_{\text{filter}} > 1$ is related to the fact, that the cross sections were calculated for $66 < m_{\ell\ell} < 116$GeV, but the generated mass range is larger. The last section of $t\bar{t}$ samples refers to variation samples for systematics studies. The MC equivalent luminosity $N_{\text{evt}}^{\text{unskim}}/(\sigma\text{·BR·}\epsilon_{\text{filter}})$ is generally above 3fb^{-1} for signal and significant backgrounds, the exception are Powheg $W \to \tau\nu$ and $Z \to \tau\tau$ samples, that have about 0.45fb^{-1} only.

Process	Data set	Generator	σ·BR·ϵ_{filter} [nb] (th. unc.)	$N_{\text{evt}}^{\text{skim}}$ [10^6]	$N_{\text{evt}}^{\text{unskim}}$ [10^6]
$Z \to \mu\mu$	364100	Sherpa 2.2.1	1.932×0.822 (5%)	8.0	8.0
$Z \to \mu\mu$	364101	Sherpa 2.2.1	1.933×0.114 (5%)	1.5	1.5
$Z \to \mu\mu$	364102	Sherpa 2.2.1	1.932×0.0660 (5%)	1.1	1.1
$Z \to \mu\mu$	364103	Sherpa 2.2.1	0.1063×0.690 (5%)	1.5	1.5
$Z \to \mu\mu$	364104	Sherpa 2.2.1	0.1062×0.200 (5%)	0.40	0.40
$Z \to \mu\mu$	364105	Sherpa 2.2.1	0.1063×0.114 (5%)	0.25	0.25
$Z \to \mu\mu$	364106	Sherpa 2.2.1	0.03889×0.593 (5%)	0.20	0.20
$Z \to \mu\mu$	364107	Sherpa 2.2.1	0.03885×0.235 (5%)	0.060	0.060
$Z \to \mu\mu$	364108	Sherpa 2.2.1	0.03889×0.156 (5%)	0.035	0.035
$Z \to \mu\mu$	364109	Sherpa 2.2.1	0.008310×0.561 (5%)	0.020	0.020
$Z \to \mu\mu$	364110	Sherpa 2.2.1	0.008310×0.266 (5%)	0.010	0.010
$Z \to \mu\mu$	364111	Sherpa 2.2.1	0.008320×0.177 (5%)	0.0050	0.0050
$Z \to \mu\mu$	364112	Sherpa 2.2.1	0.001740 (5%)	0.0050	0.0050
$Z \to \mu\mu$	364113	Sherpa 2.2.1	0.0001400 (5%)	0.0050	0.0050
$Z \to ee$	364114	Sherpa 2.2.1	1.933×0.821 (5%)	8.0	8.0
$Z \to ee$	364115	Sherpa 2.2.1	1.932×0.114 (5%)	1.5	1.5
$Z \to ee$	364116	Sherpa 2.2.1	1.932×0.0658 (5%)	1.1	1.1
$Z \to ee$	364117	Sherpa 2.2.1	0.1080×0.694 (5%)	1.5	1.5
$Z \to ee$	364118	Sherpa 2.2.1	0.1077×0.191 (5%)	0.40	0.40
$Z \to ee$	364119	Sherpa 2.2.1	0.1078×0.119 (5%)	0.25	0.25
$Z \to ee$	364120	Sherpa 2.2.1	0.03964×0.616 (5%)	0.20	0.20
$Z \to ee$	364121	Sherpa 2.2.1	0.03967×0.233 (5%)	0.060	0.060
$Z \to ee$	364122	Sherpa 2.2.1	0.04068×0.150 (5%)	0.035	0.035
$Z \to ee$	364123	Sherpa 2.2.1	0.008460×0.569 (5%)	0.020	0.020
$Z \to ee$	364124	Sherpa 2.2.1	0.008450×0.266 (5%)	0.010	0.010
$Z \to ee$	364125	Sherpa 2.2.1	0.008470×0.177 (5%)	0.0050	0.0050
$Z \to ee$	364126	Sherpa 2.2.1	0.001760 (5%)	0.0050	0.0050
$Z \to ee$	364127	Sherpa 2.2.1	0.0001451 (5%)	0.0050	0.0050

Table 12: Alternative signal $Z \to \ell\ell$ Monte Carlo samples at $\sqrt{s}$ = 13TeV produced with Sherpa. General description of the table see Table 11. The samples are split into a long list of orthogonal slices based on "max(pTV,HT)" and filtered further into "b/c/light-jet" subcomponents. For the purpose of this analysis, the number of events in each slice is such that the samples are about 2fb^{-1} each (after application of a penalty factor for negative weight events) and an "inclusive sample" is restored after merging the slices.

Process	Data set	Generator	σ·BR·ϵ_{filter} [nb] (th. unc.)	$N_{\text{evt}}^{\text{skim}}$ [10^6]	$N_{\text{evt}}^{\text{unskim}}$ [10^6]
$W \to \mu\nu$	364156	Sherpa 2.2.1	18.58 × 0.825 (5%)	31	31
$W \to \mu\nu$	364157	Sherpa 2.2.1	18.57 × 0.131 (5%)	8.1	8.1
$W \to \mu\nu$	364158	Sherpa 2.2.1	18.57 × 0.0433 (5%)	2.6	2.6
$W \to \mu\nu$	364159	Sherpa 2.2.1	0.9173 × 0.674 (5%)	6.3	6.3
$W \to \mu\nu$	364160	Sherpa 2.2.1	0.9172 × 0.244 (5%)	2.1	2.1
$W \to \mu\nu$	364161	Sherpa 2.2.1	0.9163 × 0.0847 (5%)	0.23	0.23
$W \to \mu\nu$	364162	Sherpa 2.2.1	0.3296 × 0.600 (5%)	0.80	0.80
$W \to \mu\nu$	364163	Sherpa 2.2.1	0.3297 × 0.293 (5%)	0.27	0.27
$W \to \mu\nu$	364164	Sherpa 2.2.1	0.3295 × 0.111 (5%)	0.099	0.099
$W \to \mu\nu$	364165	Sherpa 2.2.1	0.06993 × 0.548 (5%)	0.068	0.068
$W \to \mu\nu$	364166	Sherpa 2.2.1	0.06995 × 0.320 (5%)	0.034	0.034
$W \to \mu\nu$	364167	Sherpa 2.2.1	0.06991 × 0.125 (5%)	0.014	0.014
$W \to \mu\nu$	364168	Sherpa 2.2.1	0.01456 (5%)	0.020	0.020
$W \to \mu\nu$	364169	Sherpa 2.2.1	0.001200 (5%)	0.004	0.004
$W \to e\nu$	364170	Sherpa 2.2.1	18.58 × 0.825 (5%)	31	31
$W \to e\nu$	364171	Sherpa 2.2.1	18.57 × 0.131 (5%)	8.3	8.3
$W \to e\nu$	364172	Sherpa 2.2.1	18.57 × 0.0448 (5%)	2.5	2.5
$W \to e\nu$	364173	Sherpa 2.2.1	0.9168 × 0.675 (5%)	6.4	6.4
$W \to e\nu$	364174	Sherpa 2.2.1	0.9176 × 0.244 (5%)	2.1	2.1
$W \to e\nu$	364175	Sherpa 2.2.1	0.9173 × 0.0851 (5%)	0.79	0.79
$W \to e\nu$	364176	Sherpa 2.2.1	0.3295 × 0.599 (5%)	0.76	0.76
$W \to e\nu$	364177	Sherpa 2.2.1	0.3297 × 0.288 (5%)	0.28	0.28
$W \to e\nu$	364178	Sherpa 2.2.1	0.3295 × 0.111 (5%)	0.10	0.10
$W \to e\nu$	364179	Sherpa 2.2.1	0.06993 × 0.548 (5%)	0.070	0.070
$W \to e\nu$	364180	Sherpa 2.2.1	0.06996 × 0.320 (5%)	0.034	0.034
$W \to e\nu$	364181	Sherpa 2.2.1	0.06994 × 0.137 (5%)	0.014	0.014
$W \to e\nu$	364182	Sherpa 2.2.1	0.01460 (5%)	0.020	0.020
$W \to e\nu$	364183	Sherpa 2.2.1	0.001200 (5%)	0.0050	0.0050

Table 13: Alternative signal $W \to \ell\nu$ Monte Carlo samples at $\sqrt{s}$ = 13TeV produced with Sherpa. See Table 12 for a description of the table. The samples are split into a long list of orthogonal slices based on "max(pTV,HT)" and filtered further into "b/c/light-jet" subcomponents. For the purpose of this analysis, the number of events in each slice is such that the samples are about 1fb^{-1} each (after application of a penalty factor for negative weight events) and an "inclusive sample" is restored after merging the slices.

Process	Data set	Generator	σ·BR·ϵ_{filter} [nb] (th. unc.)	$N_{\text{evt}}^{\text{skim}}$ [10^6]	$N_{\text{evt}}^{\text{unskim}}$ [10^6]
$W^+ \to e^+\nu$	361100	Powheg+Pythia8	4.357 (5%)	11	11
$W^+ \to \mu^+\nu$	361101	Powheg+Pythia8	4.357 (5%)	11	11
$W^+ \to \tau^+\nu$	361102	Powheg+Pythia8	4.357 (5%)	0.065	0.94
$W^- \to e^-\bar{\nu}$	361103	Powheg+Pythia8	2.902 (5%)	7.0	7.0
$W^- \to \mu^-\bar{\nu}$	361104	Powheg+Pythia8	2.902 (5%)	7.0	7.0
$W^- \to \tau^-\bar{\nu}$	361105	Powheg+Pythia8	2.902 (5%)	0.039	0.59
$Z \to ee$	361106	Powheg+Pythia8	0.6600 × 1.025 (5%)	6.3	6.3
$Z \to \mu\mu$	361107	Powheg+Pythia8	0.6600 × 1.025 (5%)	3.4	3.4
$Z \to \tau\tau$	361108	Powheg+Pythia8	0.6600 × 1.025 (5%)	0.039	0.29
$Z \to ee$	364381	Sherpa 2.2.5	0.6600 × 1.12 (5%)	5.0	5.0
$Z \to \mu\mu$	364382	Sherpa 2.2.5	0.6600 × 1.12 (5%)	5.0	5.0
$Z \to \tau\tau$	364383	Sherpa 2.2.5	0.6600 × 1.12 (5%)	1.5	1.5
$W \to e\nu$	364384	Sherpa 2.2.5	7.259 (5%)	25	25
$W \to \mu\nu$	364385	Sherpa 2.2.5	7.259 (5%)	25	25
$W \to \tau\nu$	364386	Sherpa 2.2.5	7.259 (5%)	6.0	6.0
$ZZ(4\ell)$	361063	Sherpa 2.1	0.004624 (10%)	0.017	0.049
$WZ(\ell\ell\ell^-\nu\text{SF})$	361064	Sherpa 2.1	0.0005324 (10%)	0.0073	0.015
$WZ(\ell\ell\ell^-\nu\text{OF})$	361065	Sherpa 2.1	0.001041 (10%)	0.012	0.030
$WZ(\ell\ell\ell^+\nu\text{SF})$	361066	Sherpa 2.1	0.0008433 (10%)	0.010	0.020
$WZ(\ell\ell\ell^+\nu\text{OF})$	361067	Sherpa 2.1	0.001633 (10%)	0.016	0.039
$WW(2\ell 2\nu)$	361068	Sherpa 2.1	0.003356 (10%)	0.068	0.090
$WW(q\bar{q}\ell\nu)$	361091	Sherpa 2.1	0.006059 (10%)	0.078	0.15
$WW(\ell\nu q\bar{q})$	361092	Sherpa 2.1	0.006082 (10%)	0.14	0.26
$WZ(\ell\nu q\bar{q})$	361093	Sherpa 2.1	0.002503 (10%)	0.039	0.075
$WZ(q\bar{q}\ell\ell)$	361094	Sherpa 2.1	0.0007518 (10%)	0.017	0.025
$ZZ(q\bar{q}\ell\ell)$	361096	Sherpa 2.1	0.003789 × 0.148 (10%)	0.0070	0.010
$t\bar{t}$	410470	Powheg+Pythia8	0.06890 × 0.544 (7%)	1.8	2.8
$t(\text{s}-\text{chan.}t)$	410644	Powheg+Pythia8	0.0005400 (10%)	0.028	0.050
$t(\text{s}-\text{chan.}\bar{t})$	410645	Powheg+Pythia8	0.0002751 (10%)	0.028	0.050
Wt	410646	Powheg+Pythia8	0.002990 (10%)	0.018	0.050
$W\bar{t}$	410647	Powheg+Pythia8	0.002983 (10%)	0.019	0.050
$t(\text{t}-\text{chan.}t)$	410658	Powheg+Pythia8	0.005414 (10%)	0.028	0.050
$t(\text{t}-\text{chan.}\bar{t})$	410659	Powheg+Pythia8	0.002682 (10%)	0.028	0.050

Table 14: Monte Carlo samples at $\sqrt{s}$ = 5TeV. The table follows the same format as Table 11. The MC equivalent luminosity $N_{\text{evt}}^{\text{unskim}}/(\sigma\text{·BR·}\epsilon_{\text{filter}})$ is generally above 2.5fb^{-1} for signal and significant backgrounds, the exception are Powheg $W \to \tau\nu$ and $Z \to \tau\tau$ samples, that have about 0.20fb^{-1} and 0.45fb^{-1} only.

1.2 Multijet background

The estimate of the multijet background, which contain contributions from fake leptons produced in semi-leptonic decays of heavy quarks, in-flight pion decays, photon conversions, etc, is done using a data-driven technique. The W boson phase space is defined by the following cuts:

- $p_{\mathrm{T}}^{\ell} > 25$ GeV, $|\eta_{\ell}| < 2.4$;
- $E_{\mathrm{T}}^{\mathrm{miss}} > 25$ GeV,
- $m_{\mathrm{T}} > 50$ GeV.
- lepton isolation, using track of calorimeter-based variables.

The production of multijets is mainly concentrated at lower values of p_T^l, $E_{\mathrm{T}}^{\mathrm{miss}}$ and m_T, such that the largest part of the multijet background events are removed by the cuts described above. The background estimate is obtained by fitting the signal and multijet yields in p_T^l, $E_{\mathrm{T}}^{\mathrm{miss}}$ and m_T kinematic distributions, but with $E_{\mathrm{T}}^{\mathrm{miss}}$ and m_T cuts relaxed. These kinematic distributions for the signal are modelled using the MC simulation and include the calibrations and corrections presented in the previous chapter. The templates of the multijet distributions are obtained using the data with the same kinematic selection, but with relaxed or inverted isolation cuts. The multijet yield is obtained in the region with relaxed kinematic cuts and then extrapolated to the signal region, correcting for kinematic cuts efficiency.
First step consists in defining four different regions in phase-isolation space:

- signal region (SR): isolated leptons, signal requirement on p_T^{lep}, E_T^{miss} and m_{T};
- fit region (FR): isolated leptons, relaxed kinematic requirements: $E_{\mathrm{T}}^{\mathrm{miss}} > 0$ GeV, $m_{\mathrm{T}} > 0$ GeV;
- control region 1 (CR1): anti-isolated leptons with FR kinematic requirements;
- control region 2 (CR2): anti-isolated leptons with SR kinematic requirements.

Multijet(MJ) yield is estimated in SR. The fit region is used to perform the fraction fit, which is obtained by fitting the template obtained from the CR1. The shape of the multijet background in the SR is provided by CR2. This shape is then normalized to the ratio of MJ events in the two control regions: $\epsilon = N_{MJ}^{CR2}/N_{MJ}^{CR1}$. The number of the MJ background events is estimated in the following way:

- The number of multijet background events in CR1 (N_{MJ}^{CR1}) and their distributions (H_{MJ}^{CR1}) are derived as follows:

$$N_{\mathrm{MJ}}^{CR1} = N_{\mathrm{data}}^{\mathrm{CR1}} - N_{\mathrm{EW}}^{\mathrm{CR1}}, \tag{1.1}$$
$$H_{\mathrm{MJ}}^{CR1} = H_{\mathrm{data}}^{\mathrm{CR1}} - H_{\mathrm{EW}}^{\mathrm{CR1}} \tag{1.2}$$

where H^{CR1} stands for one of the kinematic distributions used in the fit, namely p_{T}^{ℓ}, $E_{\mathrm{T}}^{\mathrm{miss}}$ or m_{T}.

- The fraction fit is performed in FR, which has looser kinematics cuts and the same isolation cuts as the signal. The fit has the following form:

$$H_{\mathrm{data}}^{\mathrm{FR}} = \alpha \cdot H_{\mathrm{EW}}^{\mathrm{FR}} + T \cdot H_{\mathrm{MJ}}^{\mathrm{CR1}}. \tag{1.3}$$

The fitting parameter T gives the factor for the MJ contribution in FR: $N_{MJ}^{FR} \approx T \cdot N_{\mathrm{MJ}}^{CR1}$. A normalization factor for the EW+top contribution, α, is also fitted and should be unity within the uncertainties in the luminosity and the cross-sections of the MC-simulated processes.

- Then the fitted multijet yield is extrapolated to the signal region. The extrapolation factor ε that was mentioned before can be obtained as follows:

$$\varepsilon \equiv \frac{N_{\mathrm{data}}^{\mathrm{CR2}} - N_{\mathrm{EW}}^{\mathrm{CR2}}}{N_{\mathrm{data}}^{\mathrm{CR1}} - N_{\mathrm{EW}}^{\mathrm{CR1}}}, \tag{1.4}$$

and assuming that this factor does not depend in the isolation cuts, one obtains

$$N_{MJ}^{SR} = \varepsilon N_{MJ}^{FR}. \tag{1.5}$$

This method relies on the anti-isolation procedure which may introduce a bias into the results. The dependence of the MJ yield on the isolation criteria must be taken into account. In order to do this the control regions CR1 and CR2 are esimated in the slices of anti-isolation with `ptvarcone20/pT` ranging in the following intervals: [0.10, 0.15, 0.20, 0.25, 0.30, 0.35, 0.40].
The change of isolation criterion also biases the hadronic recoil reconstruction procedure, where the cone replacement appears to be isolation-dependent. This bias is overcome by introducing a correction to the hadronic recoil vector:

$$\vec{u}^{\mathrm{corr}} = \vec{u}^{\mathrm{baseline}} + \vec{u}^{\mathrm{iso}}, \text{ where} \tag{1.6}$$

$$\vec{u}^{\mathrm{iso}} \equiv \mathtt{ptcone20} \cdot \vec{n}_{\ell}. \tag{1.7}$$

The unit vector $\vec{n}_{\ell}$ is aligned with the lepton direction. This correction vanishes at low isolation in the signal region but introduces a sizable correction in the anti-isolated region (see Fig. 13). Some residual dependence of the extrapolated distributions on the isolation criteria is still present and requires shape extrapolation procedure. Distribution shape is estimated in three slices of `ptvarcone20/pT` isolation within [0.10, 0.20, 0.30 0.40] in CR2. For every observable X, $X = p_{\mathrm{T}}^{\ell}$, $E_{\mathrm{T}}^{\mathrm{miss}}$, m_{T}, the difference $\Delta[X]$ of the distribution of X between consecutive isolation slices is defined as:

$$H_{MJ}^{[0.1,0.2]}[X] = H_{data}^{[0.1,0.2]}[X] - H_{MC}^{[0.1,0.2]}[X]; \tag{1.8}$$

$$\Delta[X] = 1/2\left[(H_{MJ}^{[0.1,0.2]}[X] - H_{MJ}^{[0.2,0.3]}[X]) + (H_{MJ}^{[0.2,0.3]}[X] - H_{MJ}^{[0.3,0.4]}[X])\right], \tag{1.9}$$

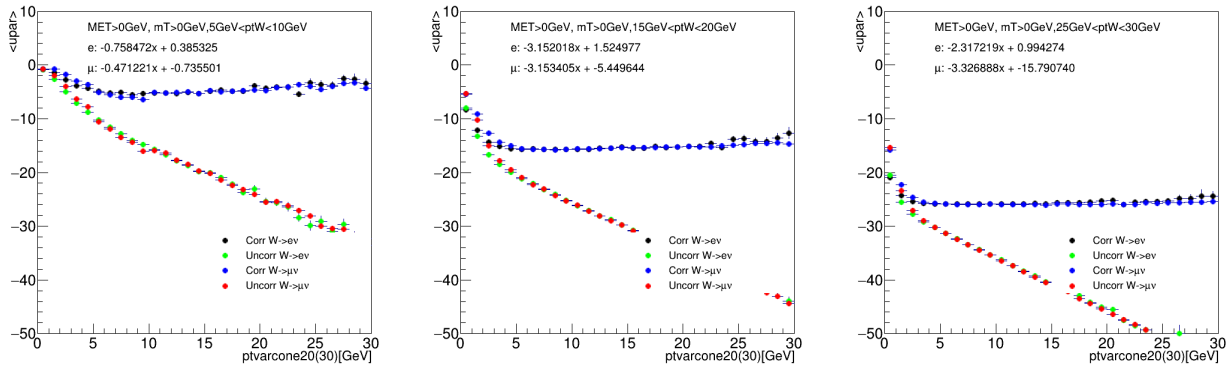

Figure 13: $< u_{\parallel}^{\ell} >$ as a function of ptcone20, before and after correction using data samples at $\sqrt{s}$ = 13 TeV.

where $H_X^{[x,y]}$ is the normalized distribution of X in CR2 (anti-isolated signal region) satisfying $x <$ ptvarcone20/pT $< y$, estimated from the MC-subtracted data in CR2.

$\Delta[X]$ is supposed to be the difference between MJ sprectrum in the signal region (ptvarcone20/pT< 0.1) and the isolation slice next to it ($0.10 <$ ptvarcone20/pT < 0.20). So the extrapolated distribution to the signal region is the following:

$$H_X^{sig} = H_X^{[0.1,0.2]} - \Delta[X] \tag{1.10}$$

The shift $\Delta[X]$ applied is assigned a 100% relative uncertainty because of large statistical uncertainty coming from the linear fit used. The MJ contributions to the kinematic distributions in slices of isolation along with the extrapolation to the signal region for the 13 TeV for electrons and muons are shown in Figures 14 and 15. The kinematic distributions with the contributions from the multijets for 5 and 13 TeV are presented in sections 1.4.3 and 1.4.2 respectively.

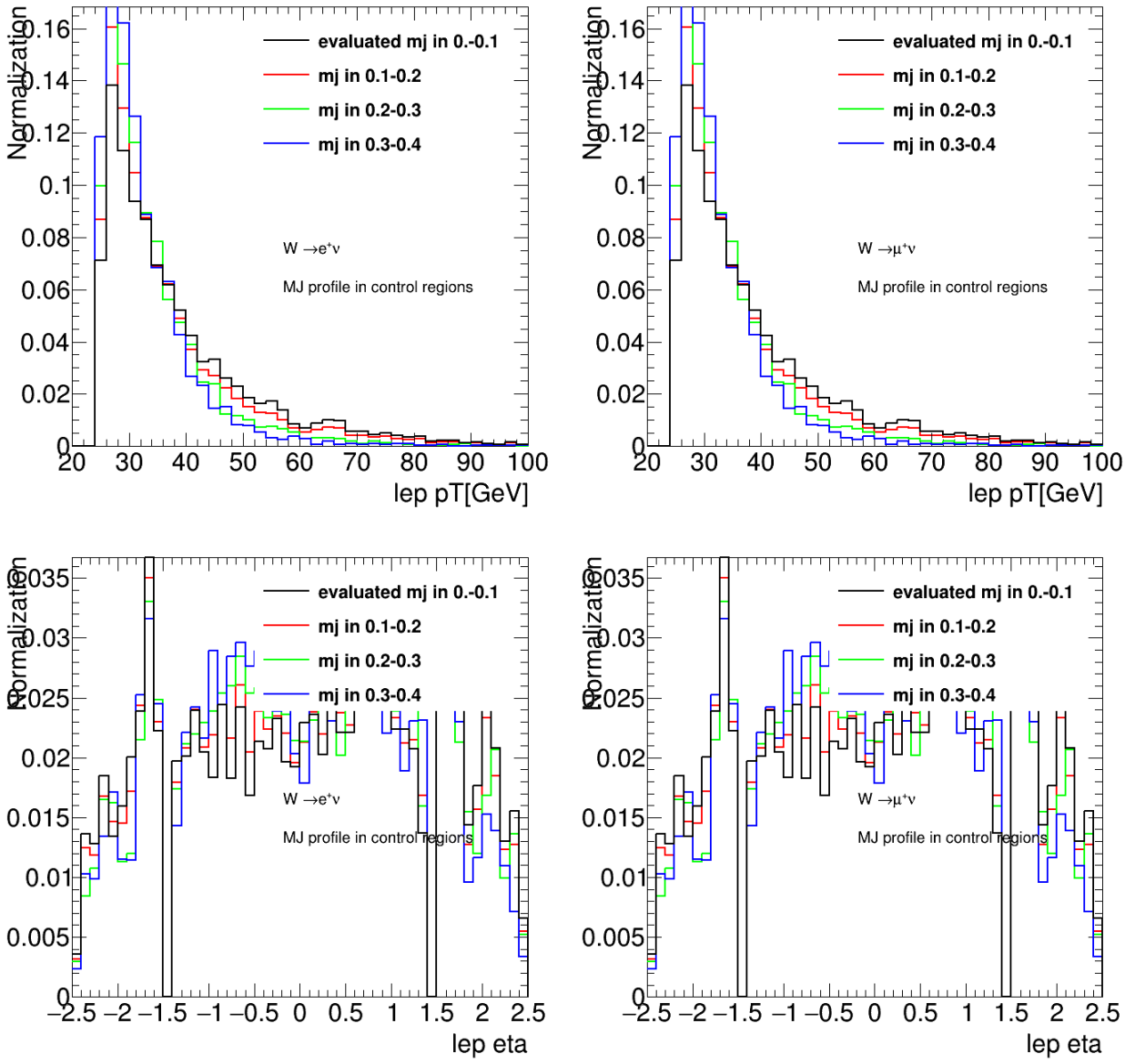

Figure 14: Extrapolation of the multijet distributions for the lepton transverse momentum (top) and pseudo-rapidity (bottom), in the $W^+ \to e^+\nu$ (left) and $W^+ \to \mu^+\nu$ (right) channels at $\sqrt{s} = 13$ TeV

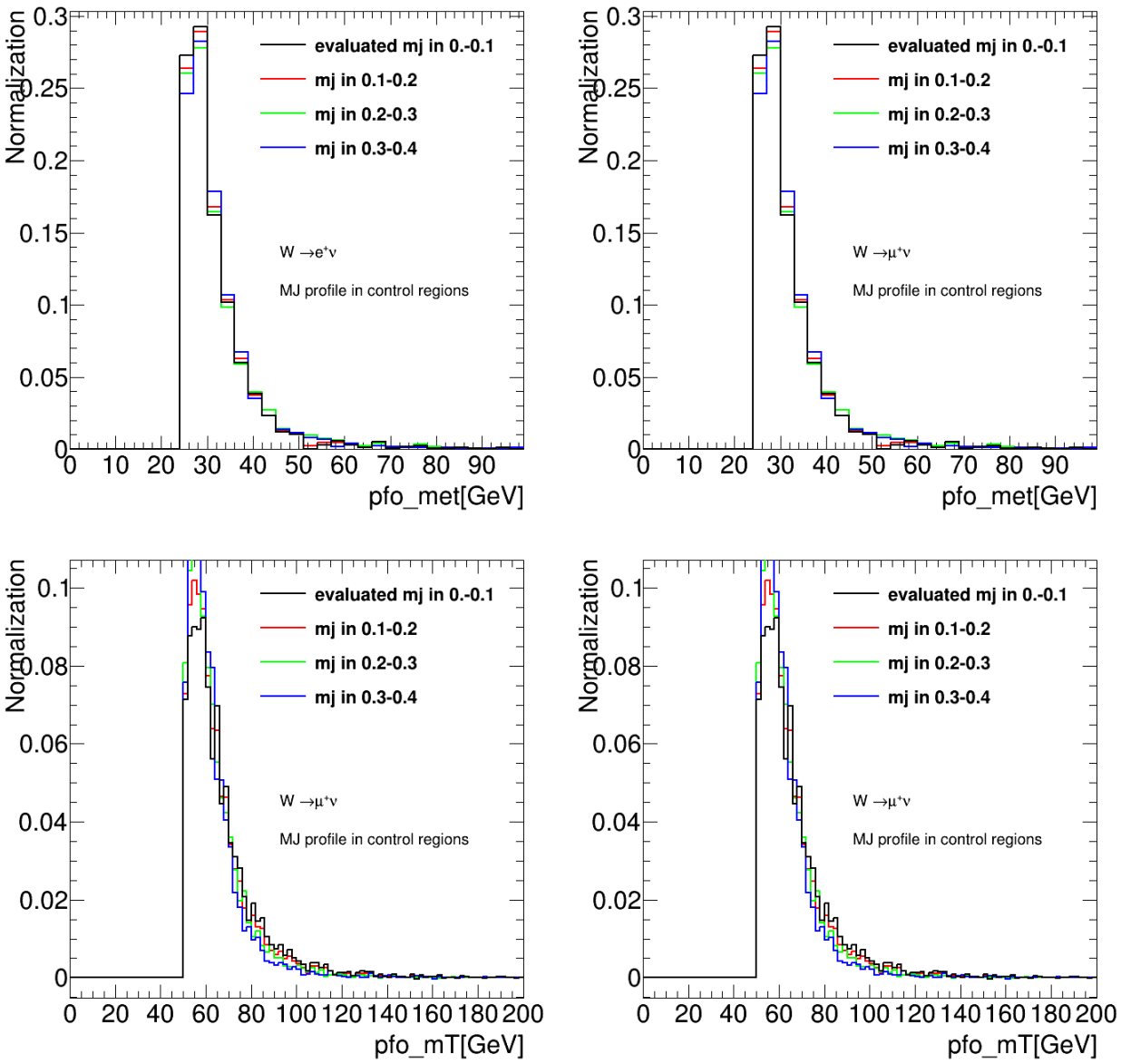

Figure 15: Extrapolation of the multijet distributions for the missing transverse energy (top) and transverse mass (bottom), in the $W^+ \to e^+\nu$ (left) and $W^+ \to \mu^+\nu$ (right) channels at $\sqrt{s} = 13$ TeV

1.3 Z vertex reweighting

The 5 TeV MC samples have been generated to be perfectly matched to the data Although this is not the case for 13 TeV samples, which can be seen at Fig. 16. It is also seen from these plots that the 2017 and 2018 data were collected at two different runs under different beam conditions. To avoid possible impact on the acceptance the MC samples were reweighted to the data using $Z \to ee$ and $Z \to \mu\mu$ selections.

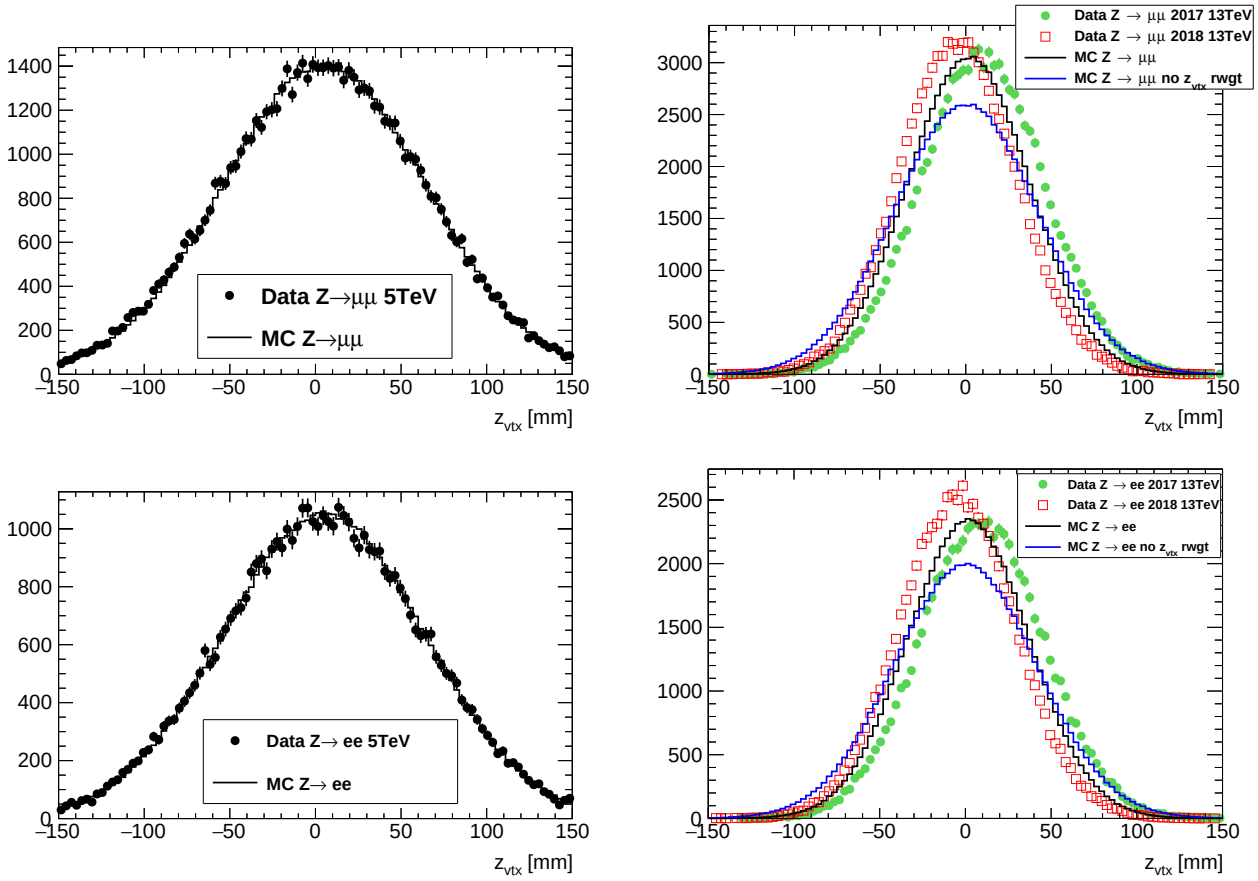

Figure 16: Distributions for the 5 TeV (left) and 13 TeV (right) low-μ dataset(s) in a $Z/\gamma^* \to \mu\mu$ (top row) and a $Z/\gamma^* \to ee$ (bottom row) selection. The data (points) is compared to $Z/\gamma^* \to \mu\mu$ or $Z/\gamma^* \to ee$ signal MC, respectively. The distributions of the z-position of the primary vertex selected as the hard interaction are compared for the dataset(s) and the MC simulation before ("no z_{vtx} rwgt", blue, only 13 TeV) and after reweighting (black). For the 13 TeV data the 2017 and 2018 data are shown separately and all distributions are (roughly) normalised to the same number of selected events in the 2017 dataset.

1.4 W analysis event selection and control plots

1.4.1 Event selection

Both in case of 5 and 13 TeV events with $W \to \ell\nu$ candidate were selected base on a single-lepton trigger requirement. The trigger for $W \to e\nu$ event candidate `HLT_e15_lhloose_nod0_L1EM12` require at least one reconstructed electron with E_{T} larger than 15 GeV passing *loose* identification requirements. Candidates for $W \to \mu\nu$ were triggered by `HLT_mu14` trigger requiring one muon with E_{T} larger than 14 GeV.

Events are required to contain exactly one lepton (muon or electron) candidate having $p_T > 25$GeV. Electrons are required to have $|\eta| < 2.47$ excluding transition region $1.37 < |\eta| < 1.52$. Muons Events with additional leptons of the same flavour with transverse momentum greater than 20 GeV satisfying some ID criteria are discarded, to better reject the Z background. The ID point is $medium$ for the muon channel, and $loose$ for the electron channel. There is no requirement on the number of leptons with different flavour than the channel under study.

To suppress background, in particular from multijet processes, events are required to have $E_{\mathrm{T}}^{\mathrm{miss}}$ greater than 25 GeV. The W boson transverse mass m_T is demanded to be larger than 50 GeV. This transverse mass is defined as follows:

$$m_T = \sqrt{2p_T^{\nu}p_T^{l}(1-\cos\Delta\phi^{\nu})} \tag{1.11}$$

The tables 15,17,19,111 contain signal selection event yields for the $W^{\pm} \to \ell^{\pm}\nu$ at $\sqrt{s} = 5$ TeV low-μ dataset. Similarly the tables 16,18,110,112 contain the corresponding numbers for the 13 TeV low-μ dataset. Table 113 provides a comparison between observed and expected yields. Events denoted as $W \to \ell\nu$ in the tables and the plots contain the sum of background events coming from $W \to \tau\nu$ and other W leptonic decays other than the signal.

Cut	Data	Signal	$W^{\pm} \to \ell^{\pm}\nu$ BG	$Z \to \ell\ell$	Top	Diboson	Multijet
One electron	1993720	643610 ± 260	32940 ± 190	44338 ± 71	1754.4 ± 3.9	772.2 ± 3.7	-
Electron trig matched	1907724	612940 ± 250	30790 ± 190	42100 ± 69	1698.5 ± 3.8	741.1 ± 3.6	-
Isolation	1438941	610320 ± 250	30590 ± 190	41923 ± 69	1663.6 ± 3.8	722.5 ± 3.6	-
$p_T^e > 25$GeV	720284	482240 ± 220	14790 ± 130	31955 ± 53	1464.5 ± 3.5	592.1 ± 3.2	-
$E_T^{miss} > 25$GeV	440605	421510 ± 210	9650 ± 100	1336 ± 20	1223 ± 3.2	420.8 ± 2.4	-
$m_T > 50$GeV	430620	417430 ± 210	8800 ± 96	1047 ± 16	944.3 ± 2.9	373.5 ± 2.2	3030 ± 550

Table 15: Analysis cut flow for $W^+ \to e^+\nu$ 5 TeV signal selection. Lepton p_{T} is required to be over 18 GeVbefore the final cut.

1.4.2 $\sqrt{s} = 13$ TeV dataset control plots

Control plots for the 13 TeV low-μ dataset are provided here after applying all corrections described in section **??**, and after applying the selection described above in this section. In each figure, the right(left)-hand column shows distributions for the W^+ (W^-) process. The top (bottom) row shows the

Cut	Data	Signal	$W^{\pm} \to \ell^{\pm}\nu$ BG	$Z \to \ell\ell$	Top	Diboson	Multijet
One electron	7915023	1797340 ± 390	92520 ± 270	147490 ± 140	63207 ± 89	3069 ± 63	-
Electron trig matched	7840239	1709140 ± 380	86370 ± 260	139760 ± 140	61110 ± 88	2967 ± 62	-
Isolation	5413483	1698430 ± 380	85560 ± 260	138890 ± 140	59834 ± 87	2939 ± 61	-
$p_T^e > 25$GeV	2452868	1342200 ± 330	44450 ± 190	106270 ± 110	53811 ± 82	2565 ± 58	-
$E_T^{miss} > 25$GeV	1275513	1136520 ± 310	28580 ± 150	8313 ± 46	45707 ± 75	1990 ± 53	-
$m_T > 50$GeV	1207776	1117560 ± 310	24760 ± 130	6443 ± 36	34580 ± 65	1718 ± 50	28000 ± 1800

Table 16: Analysis cut flow for $W^+ \to e^+\nu$ 13 TeV signal selection. Lepton p_{T} is required to be over 18 GeVbefore the final cut.

Cut	Data	Signal	$W^{\pm} \to \ell^{\pm}\nu$ BG	$Z \to \ell\ell$	Top	Diboson	Multijet
One muon	2434459	760980 ± 280	35090 ± 200	37015 ± 82	2025.3 ± 4.1	864.7 ± 3.7	-
Muon trig matched	2353403	664100 ± 260	30610 ± 190	32554 ± 76	1725.6 ± 3.8	746.6 ± 3.4	-
Isolation	1186616	659200 ± 260	30400 ± 190	32303 ± 76	1574.6 ± 3.7	710.1 ± 3.3	-
$p_T^{\mu} > 25$GeV	632016	508270 ± 230	13900 ± 130	22556 ± 57	1335.3 ± 3.4	568.2 ± 2.9	-
$E_T^{miss} > 25$GeV	470856	442600 ± 210	8700 ± 100	9959 ± 31	1111.8 ± 3	424.5 ± 2.5	-
$m_T > 50$GeV	457053	438280 ± 210	7879 ± 97	9649 ± 27	879.7 ± 2.8	381.7 ± 2.3	720 ± 190

Table 17: Analysis cut flow for $W^+ \to \mu^+\nu$ 5 TeV signal selection. Lepton p_{T} is required to be over 18 GeVbefore the final cut.

Cut	Data	Signal	$W^{\pm} \to \ell^{\pm}\nu$ BG	$Z \to \ell\ell$	Top	Diboson	Multijet
One muon	9570104	2100770 ± 410	83110 ± 270	2019400 ± 2200	71602 ± 94	3442 ± 63	-
Muon trig matched	9382783	1840550 ± 390	72820 ± 250	1750400 ± 2000	61519 ± 87	2956 ± 59	-
Isolation	3905612	1821750 ± 380	71780 ± 250	595700 ± 1100	56849 ± 84	2916 ± 59	-
$p_T^{\mu} > 25$GeV	1930655	1393330 ± 340	34470 ± 170	170840 ± 490	49338 ± 78	2471 ± 54	-
$E_T^{miss} > 25$GeV	1321407	1173860 ± 310	21450 ± 140	51090 ± 180	41956 ± 72	1930 ± 49	-
$m_T > 50$GeV	1244892	1153800 ± 310	18270 ± 130	38304 ± 81	32375 ± 63	1705 ± 44	9040 ± 800

Table 18: Analysis cut flow for $W^+ \to \mu^+\nu$ 13 TeV signal selection. Lepton p_{T} is required to be over 18 GeVbefore the final cut.

muon (electron) decay channel. In the ratio panels, the grey band is the total systematic uncertainty, whilst the brown band adds the MC statistical uncertainty in quadrature on top of it. In regions of the distributions insensitive to the modelling of p_{T}^W there is generally good agreement between data and predictions. The bulk of the m_T distribution is a typical example of distribution that is mostly insensitive to the modeling of p_{T}^W. The u_T distribution is an exception, and it can therefore be concluded that the baseline simulation is not modeling p_{T}^W satisfactorily.

Cut	Data	Signal	$W^{\pm} \to \ell^{\pm}\nu$ BG	$Z \to \ell\ell$	Top	Diboson	Multijet
One electron	1724472	374900 ± 200	24150 ± 160	41995 ± 70	1590.5 ± 2.9	684.8 ± 4	-
Electron trig matched	1645694	359010 ± 200	22070 ± 160	39854 ± 68	1539.9 ± 2.9	655.7 ± 3.9	-
Isolation	1176976	357660 ± 200	21920 ± 160	39686 ± 68	1504.6 ± 2.8	640.7 ± 3.8	-
$p_T^e > 25$GeV	529183	302070 ± 180	11920 ± 110	30214 ± 52	1330.8 ± 2.6	532.9 ± 3.5	-
$E_T^{miss} > 25$GeV	281957	266750 ± 170	8084 ± 90	1293 ± 20	1112.5 ± 2.4	380 ± 3	-
$m_T > 50$GeV	274329	264540 ± 170	7317 ± 84	994 ± 16	855.2 ± 2.1	338.1 ± 2.9	2400 ± 500

Table 19: Analysis cut flow for $W^- \to e^-\nu$ 5 TeV signal selection. Lepton p_T is required to be over 18 GeVbefore the final cut.

Cut	Data	Signal	$W^{\pm} \to \ell^{\pm}\nu$ BG	$Z \to \ell\ell$	Top	Diboson	Multijet
One electron	7471742	1323710 ± 330	78230 ± 230	140980 ± 140	61951 ± 86	3059 ± 58	-
Electron trig matched	7402574	1267710 ± 330	72240 ± 230	133580 ± 140	59950 ± 85	2968 ± 57	-
Isolation	4949352	1260540 ± 330	71550 ± 230	132740 ± 140	58689 ± 84	2937 ± 57	-
$p_T^e > 25$GeV	2113364	1053510 ± 300	39660 ± 160	101350 ± 110	52923 ± 79	2544 ± 53	-
$E_T^{miss} > 25$GeV	1008915	900640 ± 280	25900 ± 130	7954 ± 45	45065 ± 73	1962 ± 48	-
$m_T > 50$GeV	949362	887810 ± 270	22400 ± 120	6052 ± 35	34177 ± 64	1695 ± 44	27400 ± 2000

Table 110: Analysis cut flow for $W^- \to e^-\nu$ 13 TeV signal selection. Lepton p_T is required to be over 18 GeVbefore the final cut.

Cut	Data	Signal	$W^{\pm} \to \ell^{\pm}\nu$ BG	$Z \to \ell\ell$	Top	Diboson	Multijet
One muon	2075709	440560 ± 220	22510 ± 170	34440 ± 80	1835.6 ± 3.1	751.5 ± 3.3	-
Muon trig matched	2002955	383720 ± 200	19640 ± 160	30277 ± 75	1561.6 ± 2.9	648 ± 3.1	-
Isolation	883078	381010 ± 200	19450 ± 160	30046 ± 74	1411 ± 2.7	616.9 ± 2.9	-
$p_T^\mu > 25$GeV	426119	314370 ± 180	9370 ± 110	20749 ± 56	1202.1 ± 2.5	505 ± 2.5	-
$E_T^{miss} > 25$GeV	298992	276060 ± 170	5893 ± 89	8716 ± 29	1004.2 ± 2.3	372.6 ± 2	-
$m_T > 50$GeV	287870	273710 ± 170	5158 ± 82	8408 ± 26	788.2 ± 2	335.6 ± 1.9	760 ± 160

Table 111: Analysis cut flow for $W^- \to \mu^-\nu$ 5 TeV signal selection. Lepton p_T is required to be over 18 GeVbefore the final cut.

Cut	Data	Signal	$W^{\pm} \to \ell^{\pm}\nu$ BG	$Z \to \ell\ell$	Top	Diboson	Multijet
One muon	8773414	1518070 ± 360	64930 ± 230	2019900 ± 2200	70580 ± 90	3230 ± 60	-
Muon trig matched	8597493	1322980 ± 330	56520 ± 210	1750300 ± 2000	60579 ± 84	2806 ± 56	-
Isolation	3298569	1310310 ± 330	55680 ± 210	593700 ± 1100	55949 ± 80	2751 ± 55	-
$p_T^\mu > 25$GeV	1561721	1069770 ± 300	28230 ± 150	166810 ± 490	48544 ± 75	2362 ± 52	-
$E_T^{miss} > 25$GeV	1030406	910150 ± 280	17380 ± 120	47370 ± 180	41259 ± 69	1842 ± 46	-
$m_T > 50$GeV	963568	896850 ± 270	14710 ± 110	34572 ± 80	31772 ± 61	1598 ± 43	9050 ± 620

Table 112: Analysis cut flow for $W^- \to \mu^-\nu$ 13 TeV signal selection. Lepton p_T is required to be over 18 GeVbefore the final cut.

Selection	Observed	Expected
5TeV $W^+ \to e^+\nu$	430620	431620 ± 600
5TeV $W^+ \to \mu^+\nu$	457053	457790 ± 300
5TeV $W^- \to e^-\nu$	274329	276450 ± 530
5TeV $W^- \to \mu^-\nu$	287870	289160 ± 250
13TeV $W^+ \to e^+\nu$	1207776	1213000 ± 1800
13TeV $W^+ \to \mu^+\nu$	1244892	1253490 ± 870
13TeV $W^- \to e^-\nu$	949362	979500 ± 2000
13TeV $W^- \to \mu^-\nu$	963568	988560 ± 690

Table 113: Observed and Expected yield comparison for all signal selections.

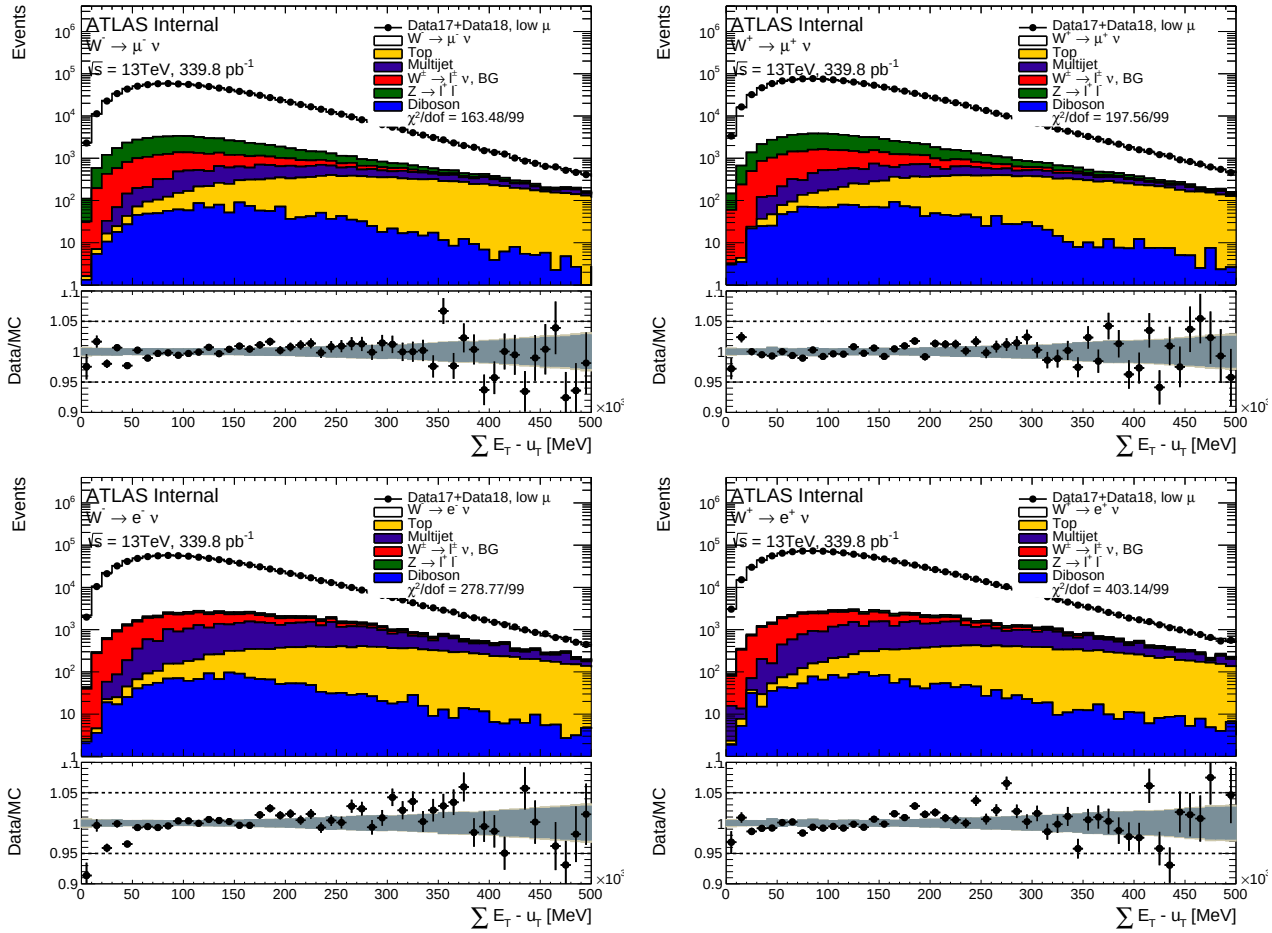

Figure 17: $\Sigma\vec{E}_T$ distribution in the muon and electron channel for the $\sqrt{s} = 13$ TeV dataset.

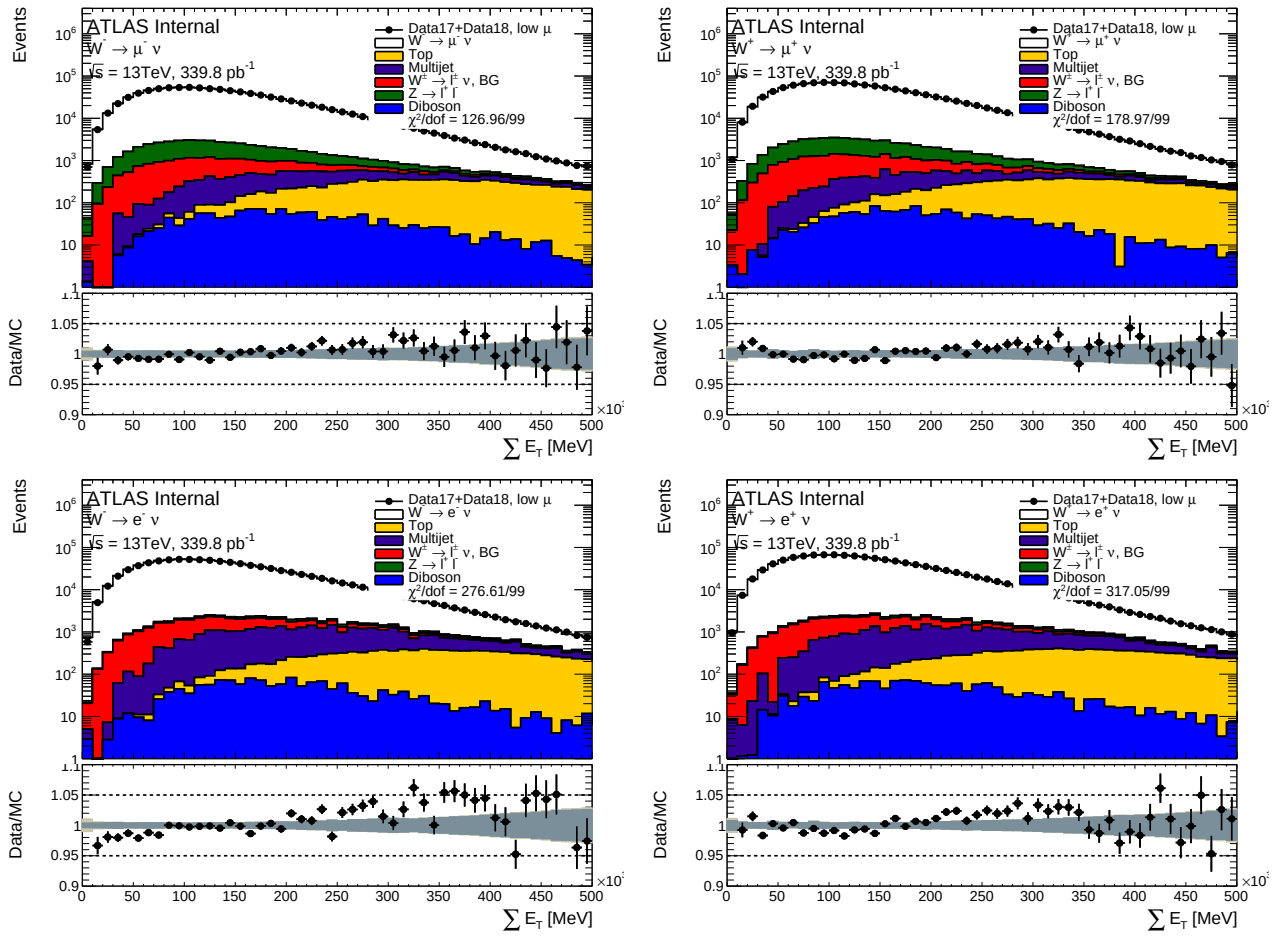

Figure 18: ΣE_T distribution in the muon and electron channel for the $\sqrt{s} = 13$ TeV dataset.

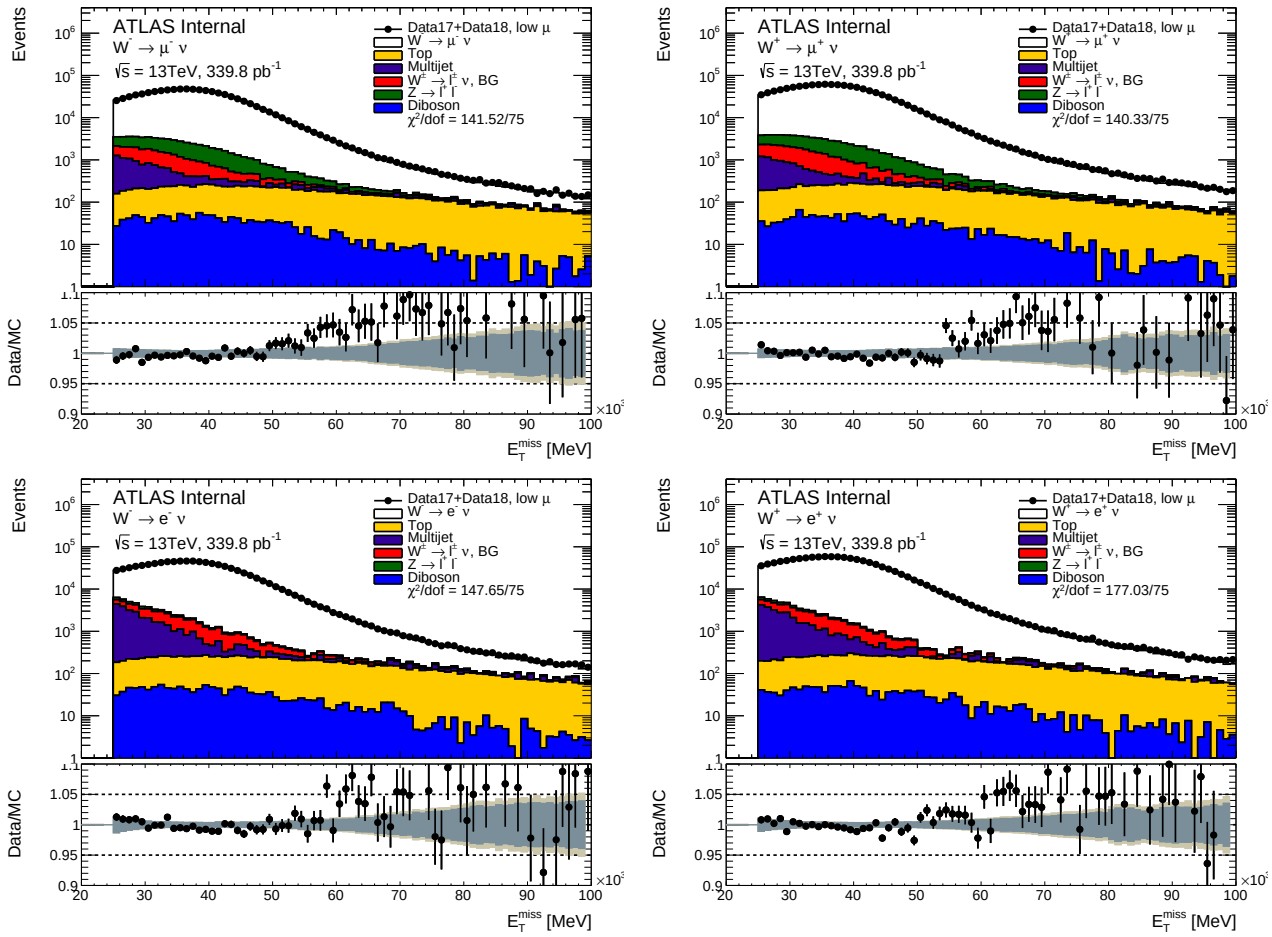

Figure 19: $\vec{E}_T^{miss}$ distribution in the muon and electron channel for the $\sqrt{s} = 13$ TeV dataset.

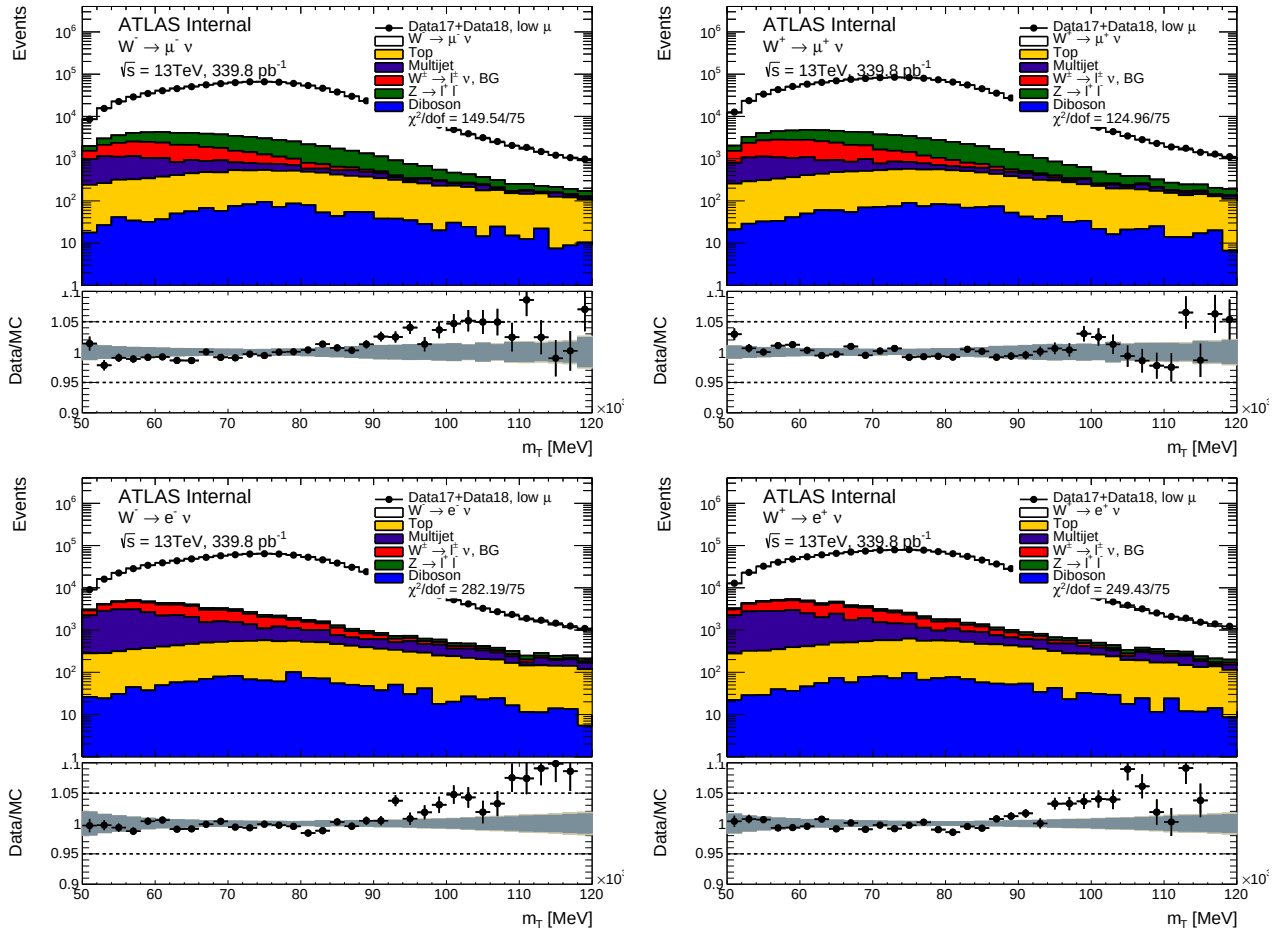

Figure 110: Transverse mass distribution of the W boson in the muon and electron channel for the $\sqrt{s} = 13$ TeV dataset.

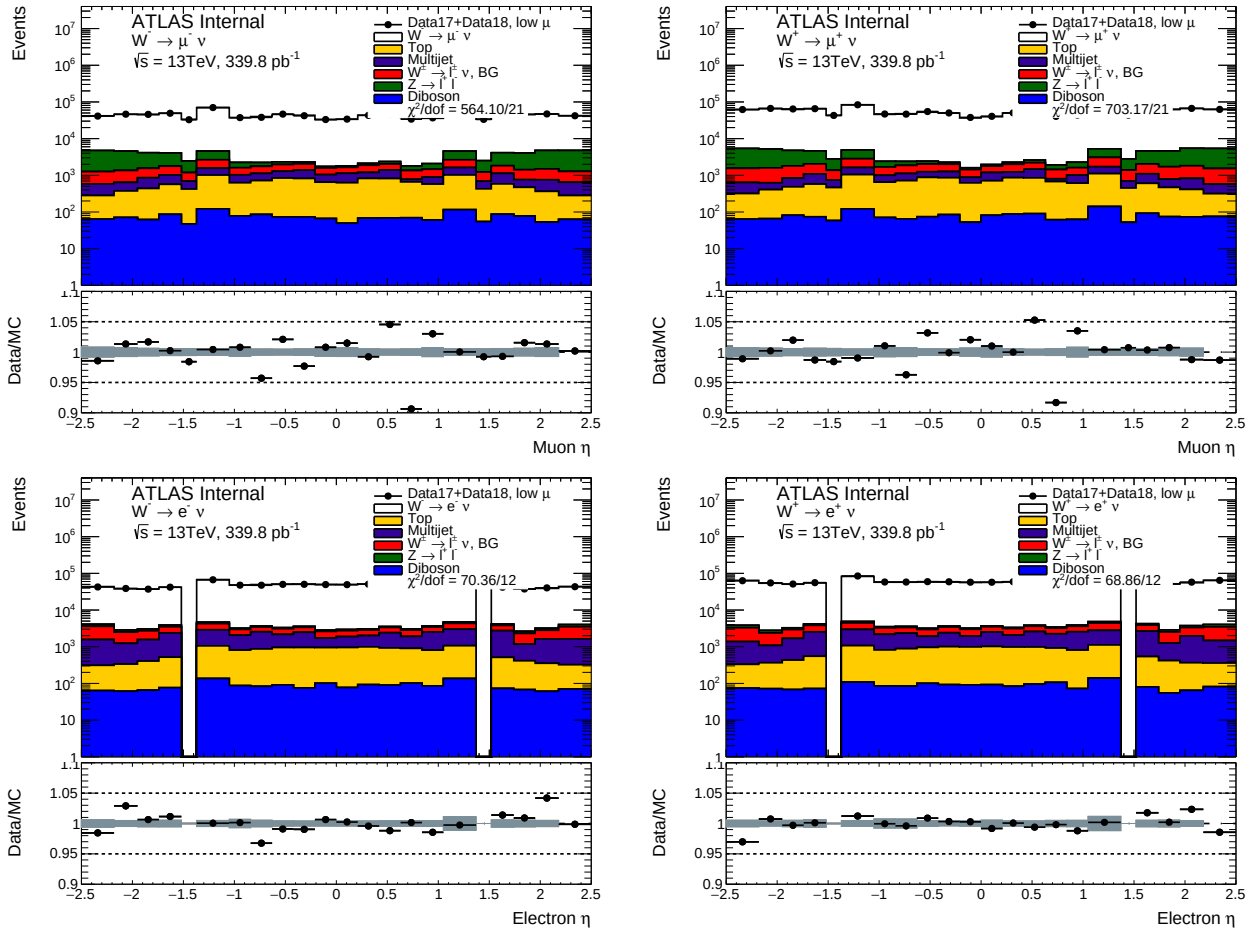

Figure 111: Lepton pseudorapidity distribution in the muon and electron channel for the $\sqrt{s} = 13$ TeV dataset.

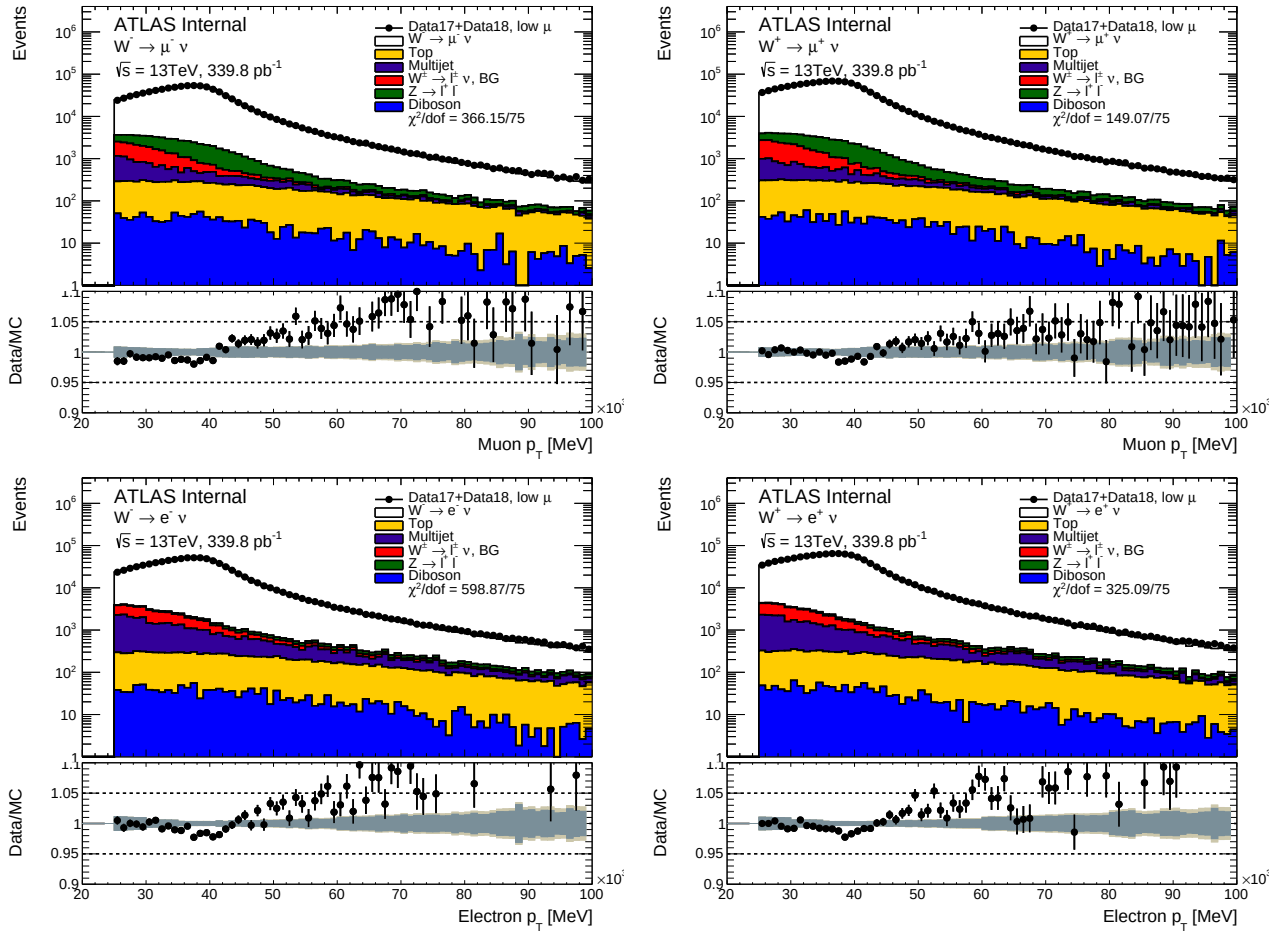

Figure 112: Lepton transverse momentum distribution in the muon and electron channel for the $\sqrt{s} = 13$ TeV dataset.

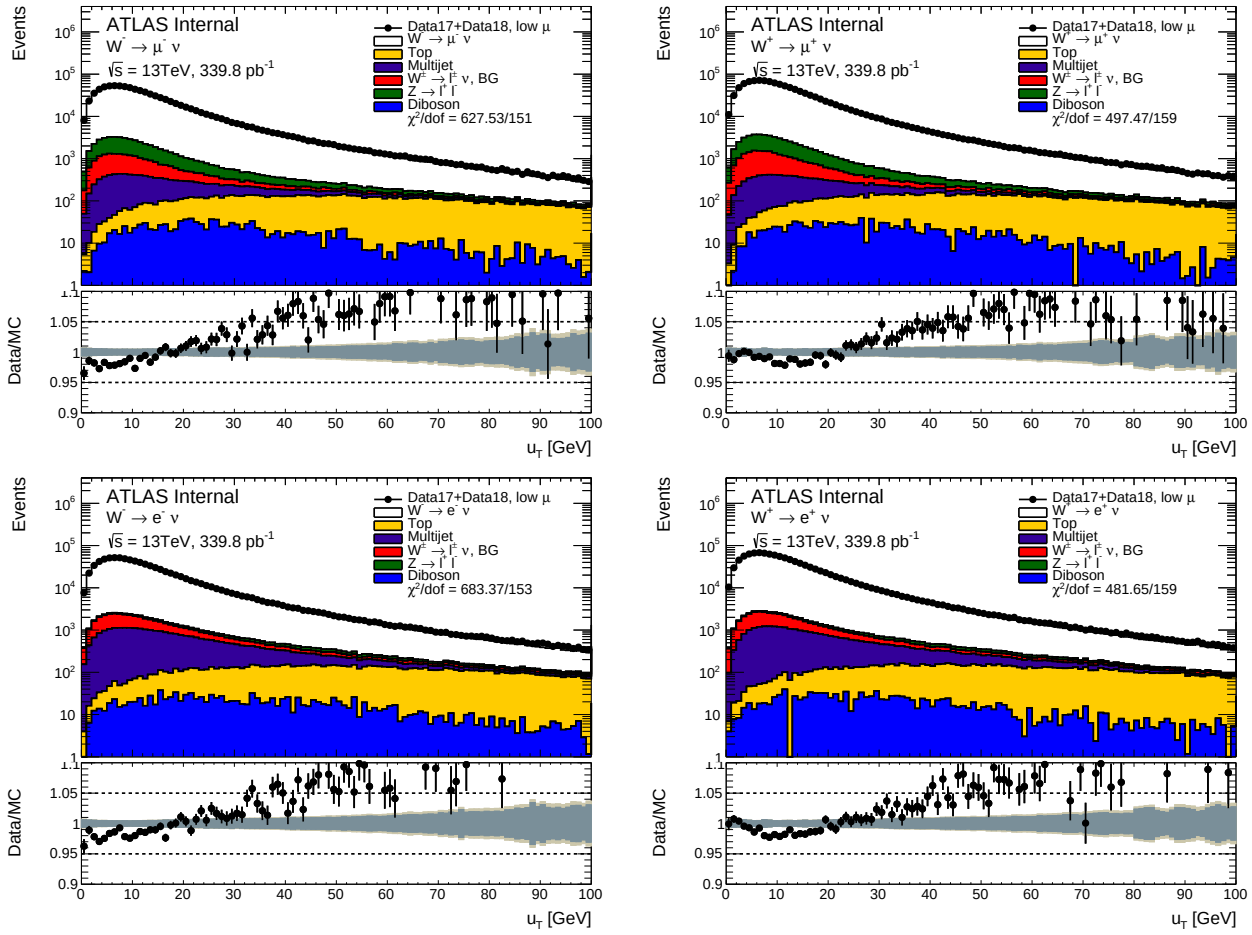

Figure 113: W transverse momentum distribution in the muon and electron channel for the $\sqrt{s} = 13$ TeV dataset.

1.4.3 $\sqrt{s} = 5$ TeV dataset control plots

Control plots for the 5 TeV low-μ dataset are provided here after applying all corrections described in section **??**, and after applying the selection described above in this section. In each figure, the right(left)-hand column shows distributions for the W^+ (W^-) process. The top (bottom) row shows the muon (electron) decay channel. In the ratio panels, the grey band is the total systematic uncertainty, whilst the brown band adds the MC statistical uncertainty in quadrature on top of it. In regions of the distributions insensitive to the modelling of p_{T}^W there is generally good agreement between data and predictions. The bulk of the m_T distribution is a typical example of distribution that is mostly insensitive to the modeling of p_{T}^W. Compared to the 13 TeV situation, the u_T distribution seems to indicate that the baseline simulation models p_{T}^W more satisfactorily.

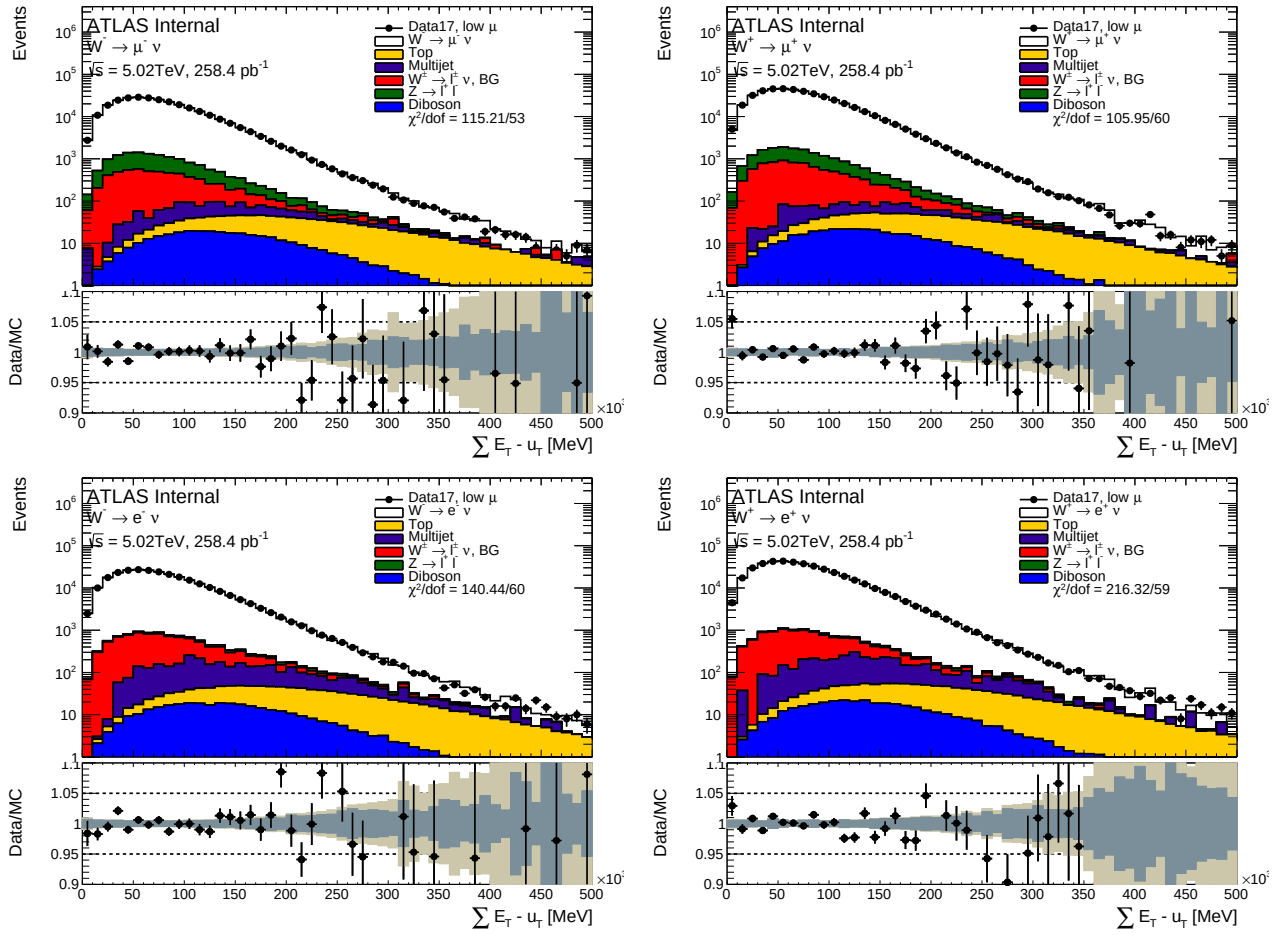

Figure 114: $\Sigma\vec{E}_T$ distribution in the muon and electron channel for the $\sqrt{s} = 5$ TeV dataset.

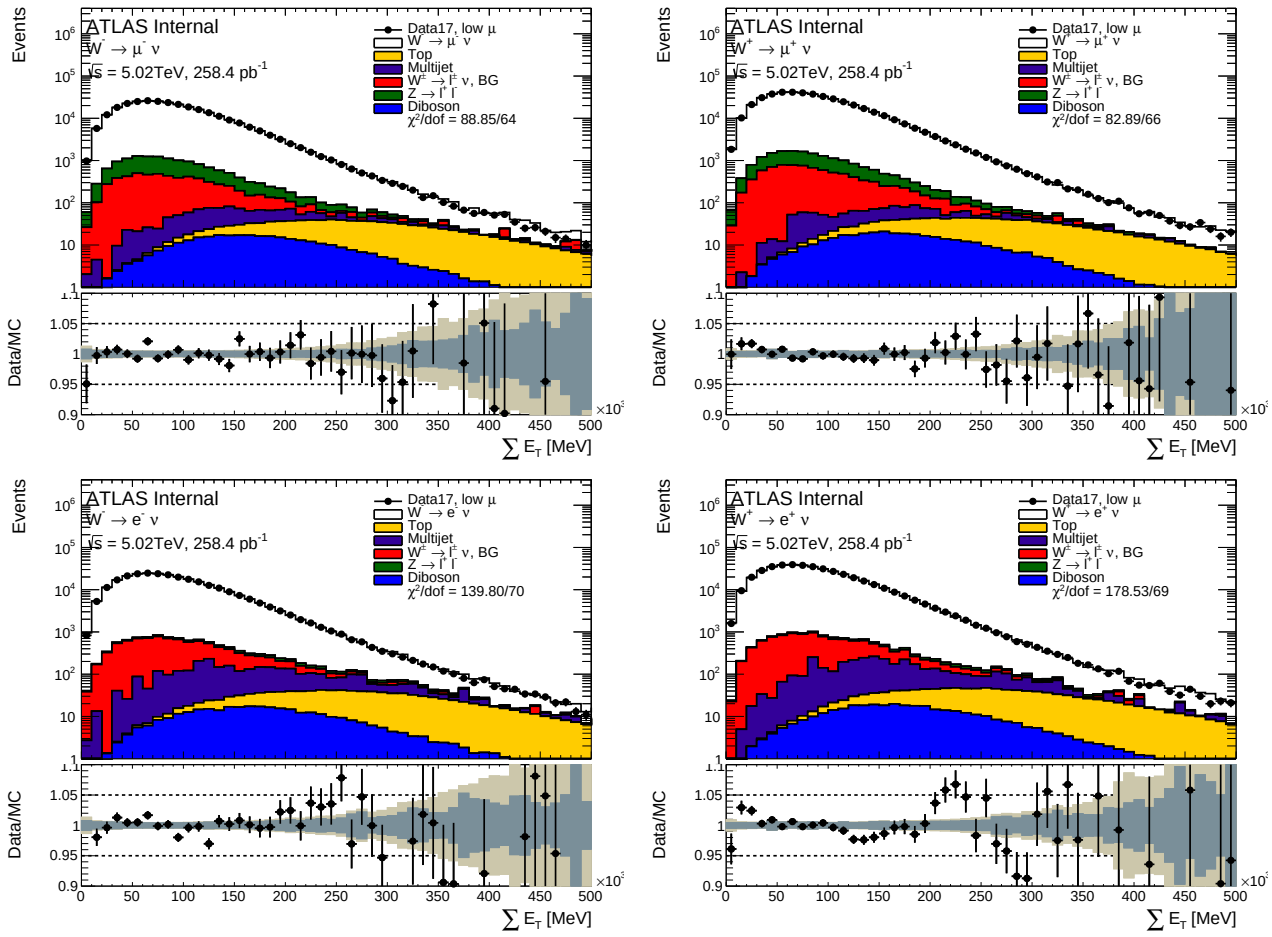

Figure 115: ΣE_T distribution in the muon and electron channel for the $\sqrt{s} = 5$ TeV dataset.

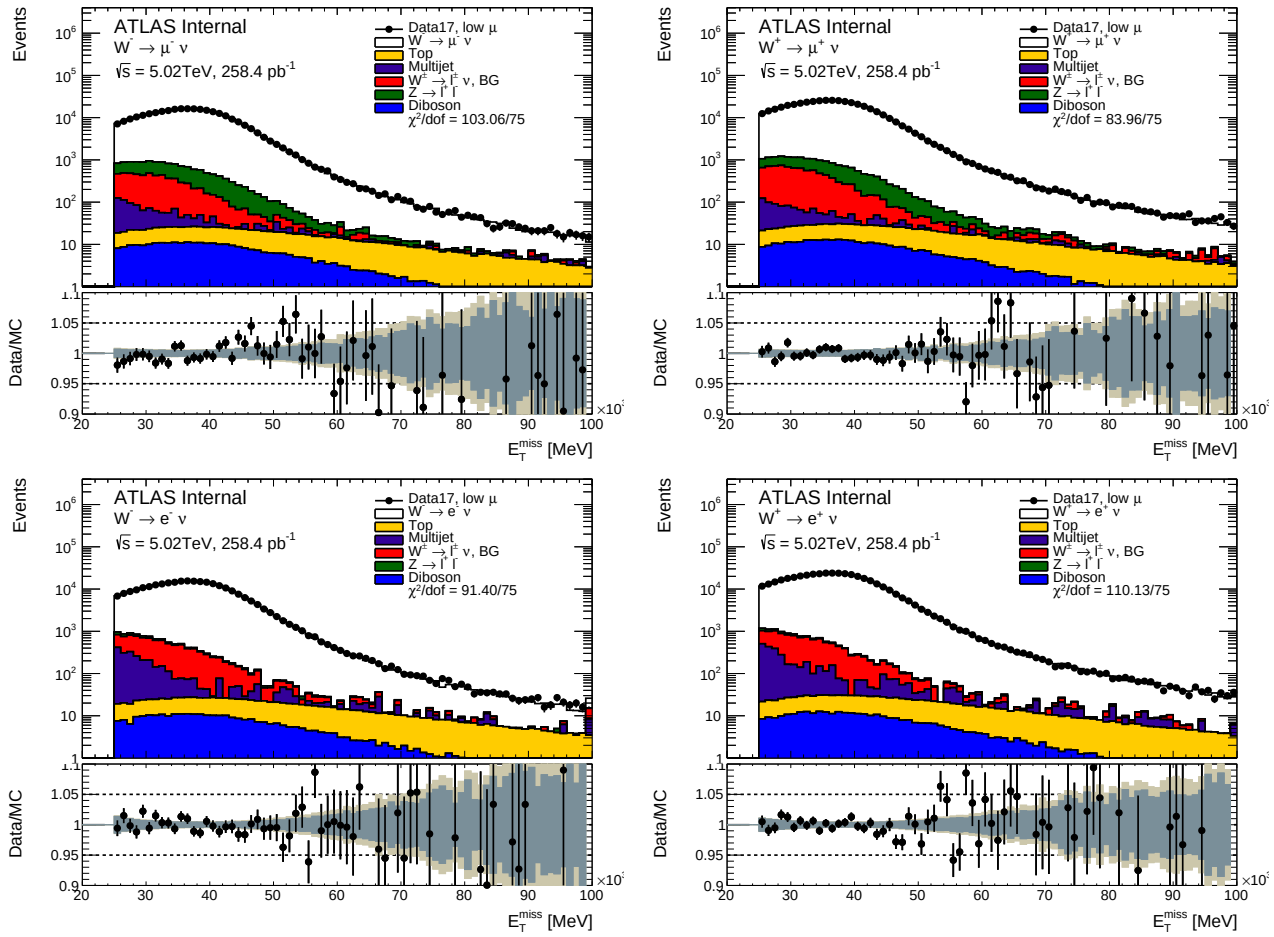

Figure 116: $\vec{E}_T^{miss}$ distribution in the muon and electron channel for the $\sqrt{s} = 5$ TeV dataset.

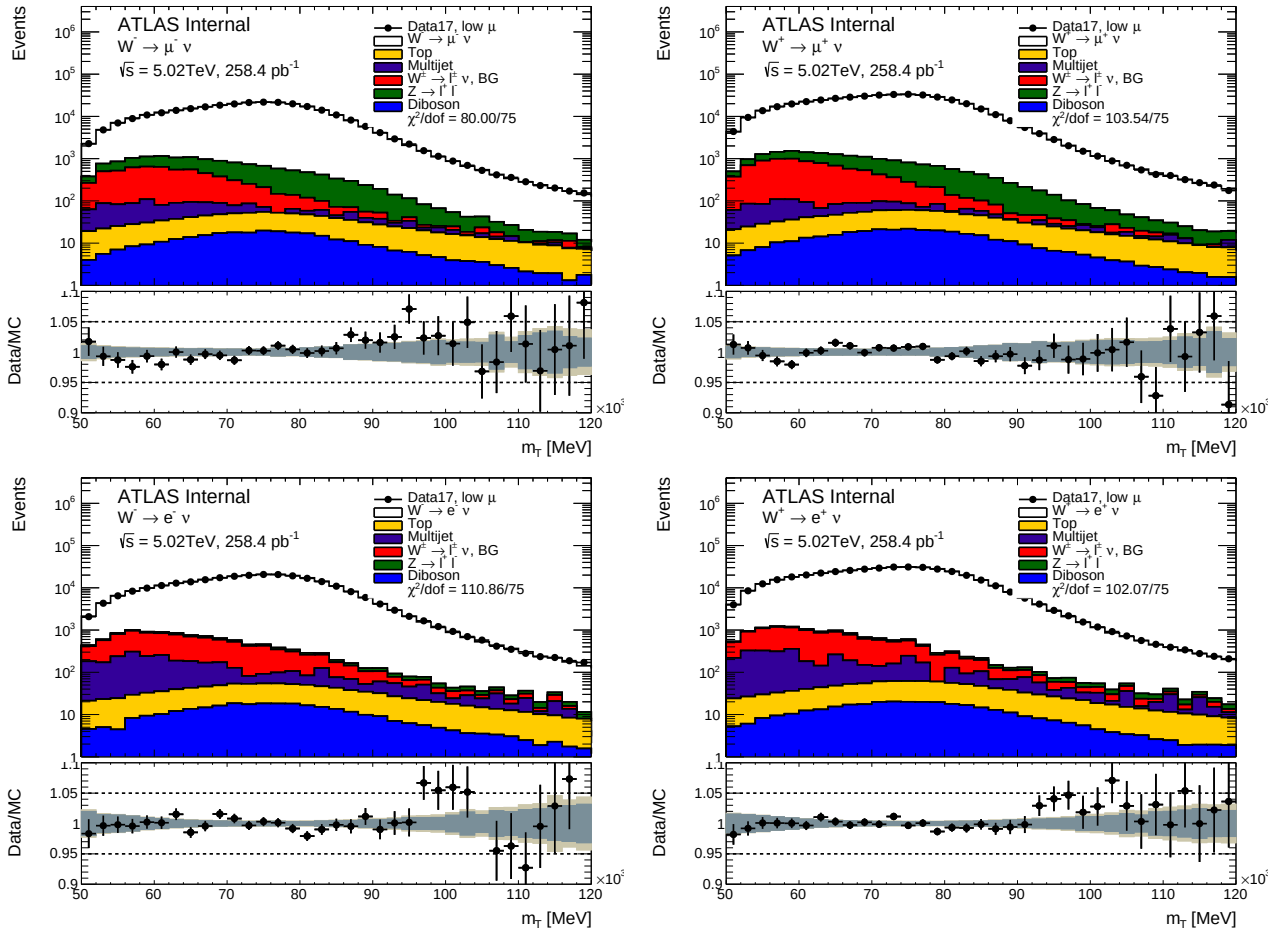

Figure 117: Transverse mass distribution of the W boson in the muon and electron channel for the $\sqrt{s} = 5$ TeV dataset.

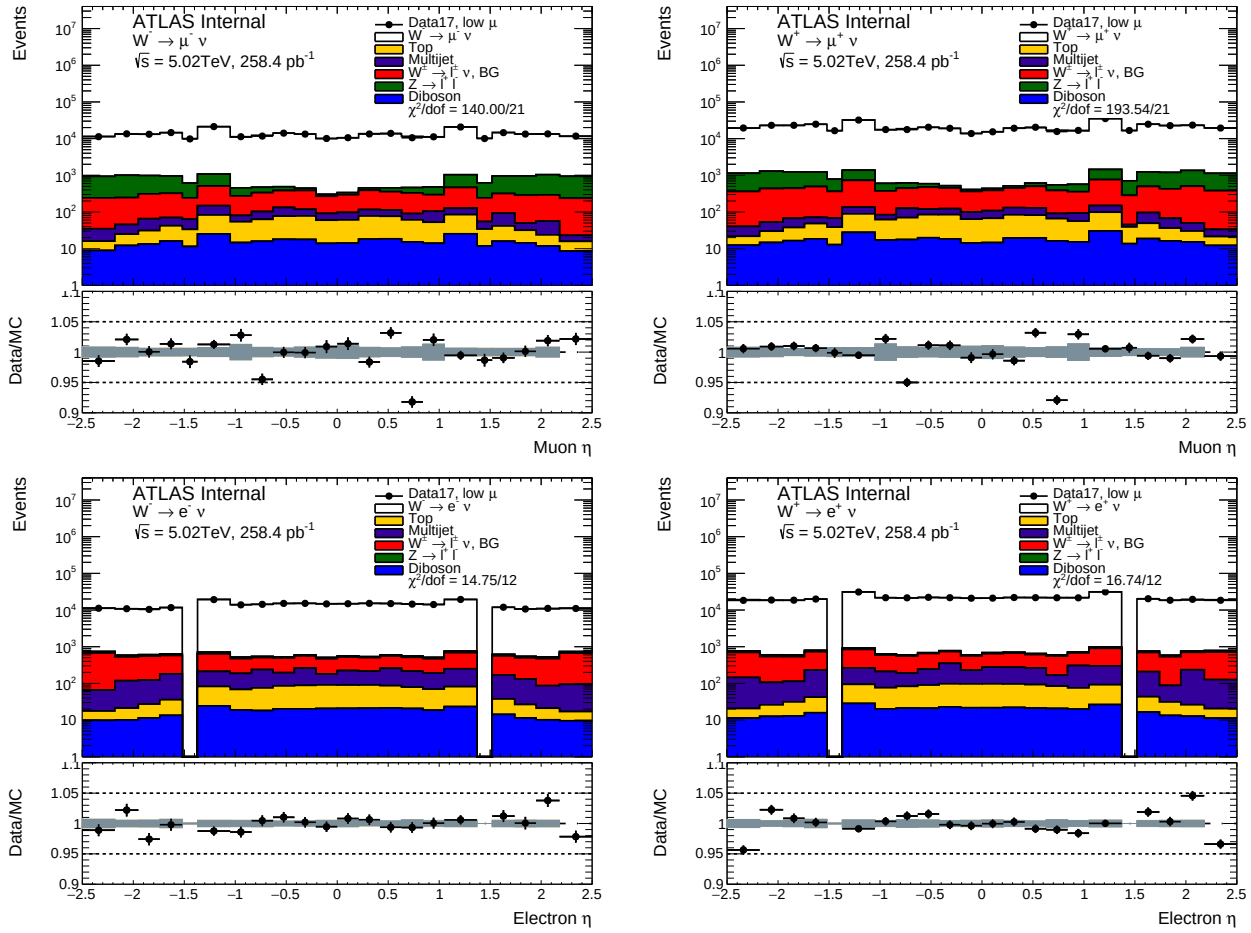

Figure 118: Lepton pseudorapidity distribution in the muon and electron channel for the $\sqrt{s} = 5$ TeV dataset.

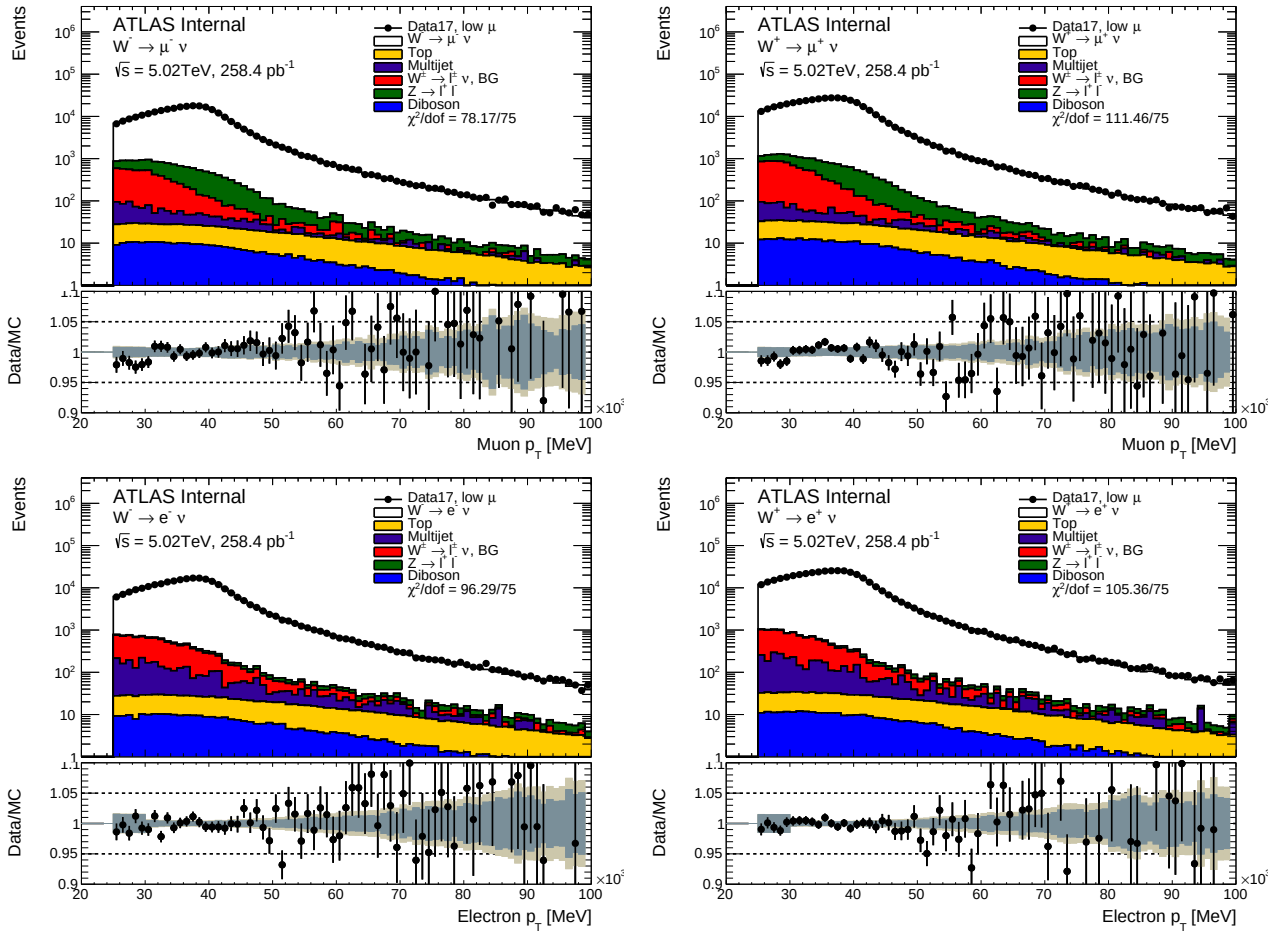

Figure 119: Lepton transverse momentum distribution in the muon and electron channel for the $\sqrt{s} = 5$ TeV dataset.

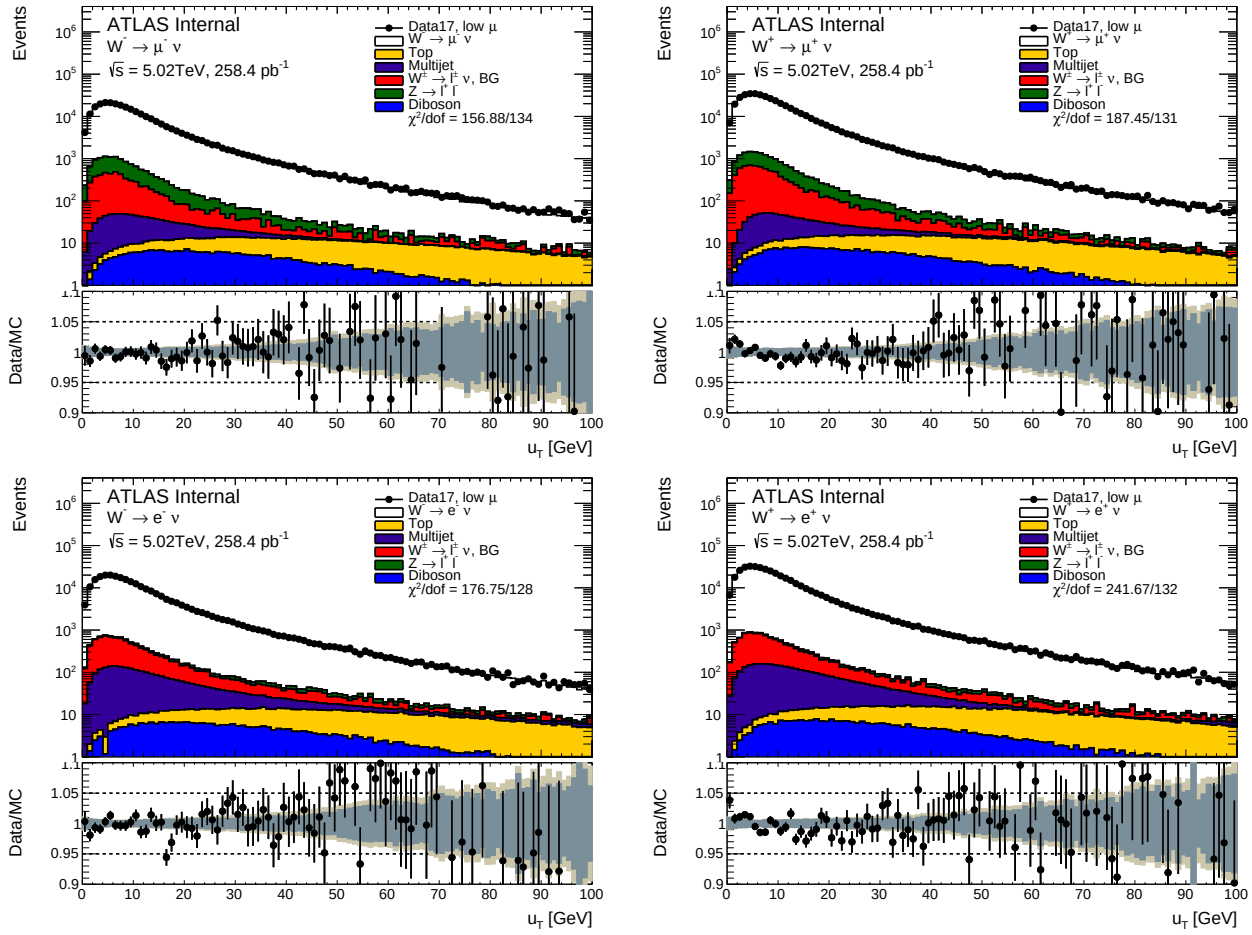

Figure 120: W transverse momentum distribution in the muon and electron channel for the $\sqrt{s} = 5$ TeV dataset.

Bibliography

[1] Jan Kretzschmar. *Samples and Physics modelling for low pile-up runs taken in 2017 and 2018*. Tech. rep. ATL-COM-PHYS-2019-075. Geneva: CERN, Feb. 2019. URL: https://cds.cern.ch/record/2657141.

[2] Paolo Nason. "A New method for combining NLO QCD with shower Monte Carlo algorithms". In: *JHEP* 11 (2004), p. 040. DOI: 10.1088/1126-6708/2004/11/040. arXiv: hep-ph/0409146.

[3] Stefano Frixione, Paolo Nason, and Carlo Oleari. "Matching NLO QCD computations with Parton Shower simulations: the POWHEG method". In: *JHEP* 11 (2007), p. 070. DOI: 10.1088/1126-6708/2007/11/070. arXiv: 0709.2092 [hep-ph].

[4] Simone Alioli et al. "NLO vector-boson production matched with shower in POWHEG". In: *JHEP* 0807 (2008), p. 060. DOI: 10.1088/1126-6708/2008/07/060. arXiv: 0805.4802 [hep-ph].

[5] Simone Alioli et al. "A general framework for implementing NLO calculations in shower Monte Carlo programs: the POWHEG BOX". In: *JHEP* 06 (2010), p. 043. DOI: 10.1007/JHEP06(2010)043. arXiv: 1002.2581 [hep-ph].

[6] T. Sjöstrand, S. Mrenna, and P. Skands. "Brief Introduction to PYTHIA 8.1". In: *Comput. Phys. Comm.* 178 (2008), p. 85. DOI: 10.1016/j.cpc.2008.01.036. arXiv: 0710.3820v1 [hep-ph].

[7] ATLAS Collaboration. "Measurement of the Z/γ^* boson transverse momentum distribution in pp collisions at $\sqrt{s} = 7$ TeV with the ATLAS detector". In: *JHEP* 09 (2014), p. 145. DOI: 10.1007/JHEP09(2014)145. arXiv: 1406.3660 [hep-ex].

[8] Piotr Golonka and Zbigniew Was. "PHOTOS Monte Carlo: A Precision tool for QED corrections in Z and W decays". In: *Eur. Phys. J.* C45 (2006), pp. 97–107. DOI: 10.1140/epjc/s2005-02396-4. arXiv: hep-ph/0506026.

[9] Stefan Höche et al. "NLO matrix elements and truncated showers". In: *JHEP* 1108 (2011), p. 123. DOI: 10.1007/JHEP08(2011)123. arXiv: 1009.1127 [hep-ph].

[10] Richard D. Ball et al. "Parton distributions with LHC data". In: *Nucl. Phys. B* 867 (2013), p. 244. DOI: 10.1016/j.nuclphysb.2012.10.003. arXiv: 1207.1303 [hep-ph].

[11] ATLAS Collaboration. *The Pythia 8 A3 tune description of ATLAS minimum bias and inelastic measurements incorporating the Donnachie–Landshoff diffractive model*. ATL-PHYS-PUB-2016-017. 2016. URL: https://cds.cern.ch/record/2206965.

[12] S. Catani and M. Grazzini. "An NNLO subtraction formalism in hadron collisions and its application to Higgs boson production at the LHC". In: *Phys. Rev. Lett.* 98 (2007), p. 222002. DOI: 10.1103/PhysRevLett.98.222002. arXiv: hep-ph/0703012 [hep-ph].

[13] S. Catani et al. "Vector boson production at hadron colliders: A Fully exclusive QCD calculation at NNLO". In: *Phys. Rev. Lett.* 103 (2009), p. 082001. DOI: 10.1103/PhysRevLett.103.082001. arXiv: 0903.2120 [hep-ph].

[14] L.A. Harland-Lang, A. D. Martin, P. Motylinski, R. S. Thorne. "Parton distributions in the LHC era: MMHT 2014 PDFs". In: *Eur. Phys. J. C* 75.5 (2015), p. 204. DOI: 10.1140/epjc/s10052-015-3397-6. arXiv: 1412.3989 [hep-ph].

[15] ATLAS Collaboration. "Measurement of $W^{\pm}$ and Z-boson production cross sections in pp collisions at $\sqrt{s}$ = 13 TeV with the ATLAS detector". In: *Phys. Lett. B* 759 (2016), p. 601. DOI: 10.1016/j.physletb.2016.06.023. arXiv: 1603.09222 [hep-ex].

[16] ATLAS Collaboration. "Measurements of W and Z boson production in pp collisions at $\sqrt{s}$ = 5.02 TeV with the ATLAS detector". In: *Eur. Phys. J. C* 79 (2019), p. 128. DOI: 10.1140/epjc/s10052-019-6622-x. arXiv: 1810.08424 [hep-ex].

[17] CMS Colaboration. "Measurement of the inclusive $t\bar{t}$ cross section in pp collisions at $\sqrt{s}$ = 5.02 TeV using final states with at least one charged lepton". In: *JHEP* 03 (2018), p. 115. DOI: 10.1007/JHEP03(2018)115. arXiv: 1711.03143 [hep-ex].